Mössbauer Spectroscopy of Iron Oxide Nanoparticles: Materials for Biomedical Applications

A Dissertation Presented for the

Doctor of Philosophy

Degree

The University of Tennessee, Knoxville

Hien-Yoong Hah

December 2018

Copyright © 2018 by Hien-Yoong Hah

All rights reserved.

ACKNOWLEDGEMENTS

I would like to acknowledge all the hard work that my parents did, my mother in particular, in getting all of us (me and my siblings) this far. Along this journey, she has both contributed and suffered the most, always with dignity and receiving little praise and acknowledgement. My siblings and my father often are the ones keeping me honest and motivated, be it by example, advice or expectation.

I would also like to thank my committee members, Dr Jackie Johnson, Dr Saeed Kamali, Dr Claudia Rawn and Dr Feng Yuan Zhang for generously allocating time to read, edit and critique my writing.

In academic terms, I would like to thank Dr Jackie Johnson for her tireless edits of my numerous writings and providing me the opportunity to pursue my PhD. Dr Charles Johnson on the other hand provided me with an inexhaustible source of scientific, philosophical and cultural knowledge, while also constantly instructing me in the proper methods of scientific inquiry. Frequently, he filled in the gaps in my knowledge, knowledge that I had taken for granted and scarcely thought twice about. Dr Saeed's good food and good company constantly reminded me of the kindness that is needlessly absent in this world, and showed me that kindness does not come at the expense of the self. More importantly he personifies the quote "the true measure of a person is how he treats those who can do nothing for him".

Special thanks to Doug Warnberg, Alexander Terekhov and Kathleen Lansford, the technical staff at UTSI that enabled our daily activities in the lab. In particular, Alexander and Doug had the unfortunate pleasure of being the persons for repairs and technical questions. Many a time, I occupied their time and expertise with both those issues.

My mates, Chad Bond, Adam Evans and Julie King who were on this academic journey all helped me at various times, with Adam helping with car repairs, and Julie frequently treating us to good food.

Lastly for the many persons that have helped me and whom I did not mention, please forgive me and know that it is not out of lack of appreciation, but poor memory that I have left you out. I deeply appreciate each and every one of you. Thank you.

ABSTRACT

Nanoparticles of Fe_3O_4 (magnetite) and gamma-Fe_2O_3 (maghemite) have been studied by Mössbauer spectroscopy. These nanoparticles have applications as contrast agents for Magnetic Resonance Imaging. At room temperature, they are superparamagnetic and the magnetic hyperfine fields were averaged to zero. The spectra of Fe_3O_4 were composed of two lines corresponding to two crystal sites, identified from their isomer shifts as Fe^{3+} on the tetrahedral A site and $Fe^{2.5+}$ (mixed Fe^{2+} and Fe^{3+}) on the octahedral B site. The relative intensity of the two lines shows that the samples are almost stoichiometric with the formula $Fe_{3-x}O_{4,}$ where x is less than 0.04 at room temperature. The x that was obtained was compared to those obtained in a magnetic field and at room temperature. The lines are broad and the measurements as a function of temperature were analyzed using Néel's theory of superparamagnetism to yield values of the relaxation times. The same nanoparticles that have oxidized into gamma-Fe_2O_3 have been studied for comparison.

TABLE OF CONTENTS

Chapter 1 Introduction 1
Magnetic Nanoparticles 1
Iron Oxide Nanoparticles and Medical Applications 1
General Information 3
Iron Oxide 3
Verwey Transition 4
Stoichiometry 4
Magnetism 5
Curie Temperature 7
Larmor Precession 7
Superparamagnetism 8
Magnetic Anisotropy 8
Blocking Temperature 9
Mössbauer Spectroscopy 9
Low Temperature Experiments 10
Isomer Shift 11
Quadrupole Splitting 11
Magnetic Hyperfine Field 12
Linewidth 13
Motional Narrowing 13
Chapter 2 Experimental Methods 14
Synthesis of Iron Oxide Nanoparticles 14
Characterization 14
TEM 14
XRD 15
Mössbauer Spectroscopy 15
The Source 15
The Detector 15
The Sample 16
Experiments in External Magnetic Field 17

Low Temperature Experiments 17
Fitting Methods 19
Chapter 3 Results and Discussion 20
Mössbauer spectroscopy: Bulk magnetite and maghemite 20
Stoichiometry: Qualitative and Quantitative Analysis 20
Low Temperature Experiments 25
Low Temperature Experiments: Stoichiometry 28
Room Temperature Experiments: Stoichiometry 29
Magnetic Field Experiments 31
Magnetic Field Experiments: Stoichiometry 38
Blocking Temperature and Superparamagnetism 40
Relaxation Time: A Motional Narrowing Analysis 40
Assumptions 44
Analysis 44
Motional Narrowing: Limitations 47
Chapter 4 Conclusion 49
References 50
Vita 54

LIST OF TABLES

Table 1 Low temperature hyperfine parameters. 27
Table 2 Low temperature percentages of iron species of initial samples. 28
Table 3 Room temperature percentages of iron species of initial samples. 29
Table 4 In magnetic field percentages of iron species of initial samples. 38
Table 5 Comparison of the x values for room temperature, in magnetic field and low temperature. 39
Table 6 Nanoparticle relaxation times. 45
Table 7 The characteristic relaxation times and blocking temperature of the particles. 47

LIST OF FIGURES

Figure 1 Magnetite tetrahedral and octahedral structure 4
Figure 2 Magnetic moments in a paramagnet. 6
Figure 3 Magnetic moments in a ferromagnet. 6
Figure 4 Magnetic moments in a ferrimagnet. 7
Figure 5 Magnetic moments in antiferromagnet. 7
Figure 6 A magnetic moment precessing around a magnetic field. 8
Figure 7 The nuclear transitions of the sample. 11
Figure 8 The effect of magnetic dipole splitting on the energy levels. 12
Figure 9 TEM of 5.3 nm iron oxide nanoparticles. 14
Figure 10 Mössbauer experimental setup. 15
Figure 11 The pulse height spectrum on the Mössbauer detector. 16
Figure 12 Sample holder for the iron oxide nanoparticles. 17
Figure 13 The 20 kG magnet, the sample is placed in the hole during experiments. 17
Figure 14 The cryostat with the Mössbauer setup. 18
Figure 15 Bulk magnetite and maghemite at room temperature. 21
Figure 16 Bulk forms of magnetite and maghemite. 22
Figure 17 Mössbauer spectra of iron oxide nanoparticles, magnetite nanoparticles at room temperature. 23
Figure 18 Mössbauer spectra of maghemite nanoparticles, at room temperature. 24
Figure 19 Mössbauer spectra of magnetite nanoparticles, initial experiments at 6 K. 26
Figure 20 Mössbauer spectra of maghemite nanoparticles, at 6 K. 27
Figure 21 Mössbauer spectra of iron oxide nanoparticles, initial experiments at room temperature 30
Figure 22 Mössbauer spectra of iron oxide nanoparticles, initial experiments in 10 kG magnetic field at room temperature. 32
Figure 23 Mössbauer spectra of maghemite nanoparticles in 10 kG magnetic field at room temperature. 33
Figure 24 Mössbauer spectra of 10.6 nm sample in 10 kG magnetic field at room temperature. 35

Figure 25 Mössbauer spectra of magnetite nanoparticles, initial experiments in 20 kG magnetic field at room temperature. 36
Figure 26 Mössbauer spectra of maghemite nanoparticles, in 20 kG magnetic field at room temperature. 37
Figure 27 Mössbauer spectra of the 10.6 nm sample in 20 kG magnetic field at room temperature. 39
Figure 28 The initial varying temperature experiments of magnetite samples 5.3 nm, 8.6 nm and 10.6 nm. 41
Figure 29 The varying temperature experiments of maghemite samples 5.3 nm, 8.6 nm and 10.6 nm. 42
Figure 30 Plot of $ln\ \tau$ against 1/T for initial unoxidized magnetite 5.3 nm, 8.6 nm and 10.6 nm nanoparticles. 46
Figure 31 Plot of $ln\ \tau$ against 1/T for maghemite 5.3 nm, 8.6 nm and 10.6 nm nanoparticles. ... 46

Chapter 1 Introduction

This thesis work is focused on superparamagnetic iron oxide nanoparticles (SPIONs) that are non-stoichiometric. Magnetite, has stoichiometry Fe_3O_4. However it is often non-stoichiometric and oxidizes into other forms of oxides, most notably maghemite (γ-Fe_2O_3). The non-stoichiometry carries over in its nanoparticle form. The high surface area-to-volume ratio in nanoparticles increases the predisposition to oxidation in comparison to the bulk, making some SPIONs completely maghemite. Mössbauer spectroscopy is the predominat characterization method for superparamagnetic iron oxide nanoparticles presented here.

Magnetic Nanoparticles

Bulk compounds of iron, nickel or cobalt are frequently magnetic. SPIONs, largely composed of iron, are magnetic and therefore interact with an external magnetic field. Since the magnetism of the SPIONs feature heavily in applications, it is important to understand it. Magnetic nanoparticles have been used for memory storage, nanofluids, waste water treatment and catalyst supports[1]. Medical applications of materials are becoming more important, with the increased longevity of people resulting in the need for healthcare. The medical applications of SPIONs include their use as contrast agents in medical imaging as well as in cancer therapy through magnetic hyperthermia[2].

Iron Oxide Nanoparticles and Medical Applications

SPIONs consist of an iron oxide core with a coating. Typically, this iron oxide core is magnetite or maghemite, with a coating of polyethylene glycol (PEG), polyvinyl alcohol (PVA) or silica[3]. Sometimes, this coating can be another layer of iron oxide[4]. All these coatings function as a barrier to further oxidation of the nanoparticles. SPIONs with coatings have been found to have low toxicity in humans, increasing their viability for applications within the human body [5,6].

In cancer therapy, SPIONs that are specifically functionalized can be used for targeted drug delivery. During treatment, cancerous sites can be targeted with the use of an external magnetic field. This is in contrast with many current drug therapies that suffer from being non-specific to the region of interest. This non-specificity requires patients to receive large doses of a drug to achieve the required concentration at the cancerous sites, which can lead to harmful side effects. Using SPIONs, heat can be generated through the application of radio frequencies, destroying the cancerous cells[7]. Furthermore, unlike many drugs, working on nanoscales allow SPIONs to be

small enough to cross the blood-brain barrier[8]. This increases their potential in treating brain tumors.

The potential of SPIONs in cancer therapies cannot be overstated; the second leading cause of death in the US population is cancer, according to the Centers for Disease Control and Protection (CDC), and improving cancer therapy outcomes for patients is of paramount importance[9].

Magnetic Resonance Imaging (MRI) contrast agents, like Gadolinium and SPIONs, work by modifying the relaxation time[10]. These relaxations contribute to the signal-to-noise ratio in an image. Specifically, it is the difference in the relaxations in each organ/tissue that provides the contrast in an MRI image. Each molecule in the human body carries a small magnetic dipole, which originates from the proton in the hydrogen atom. During the acquisition of an image, an external magnetic field is applied and magnetic dipoles will align themselves to the field. Once the external field is removed, the magnetic dipoles will "relax" back to their unexcited positions and the time that is taken to return to the original positions is termed the "relaxation time". When using a contrast material like SPIONs, the magnetic dipoles from the nanoparticles themselves can modify the relaxation time of the molecules in the body. However, it is found that the numerous examples of SPIONs reported in the literature are either not superparamagnetic at room temperature or not stoichiometrically magnetite[11,12,13]. Magnetite has a larger magnetic moment than that of maghemite making it potentially better for medical purposes, as lower concentrations of it will be needed in the human body. The superparamagnetism of the SPIONs is important as it correlates to the relaxation time when used as an MRI contrast agent[14,15]. As a result, properly characterizing the stoichiometry and magnetic properties of SPIONs become important.

In this dissertation, our collaborators at Xavier University in Louisiana successfully synthesized SPIONs that are almost stoichiometric magnetite. At UTSI, Mössbauer Spectroscopy experiments performed at variable temperature and in external magnetic fields have been used to characterize these nanoparticles. Some characterization of the magnetite nanoparticles had been done in previous thesis work[16]. For the dissertation work here, the oxidized nanoparticles, which is stoichiometrically maghemite have been characterized. Firstly, motional narrowing, a technique common in nuclear resonance imaging, is proposed as a model for understanding the relaxation of these nanoparticles. Secondly, room temperature Mössbauer spectra, which are less valued due to the absence of a hyperfine field in some nanoparticles are fitted with a model similar to those above

the Curie temperature. The validity of these models will be justified by comparing the results to other well-established techniques.

General Information

The historical impact of iron, in its many forms, has been huge. Although having existed and wrought by ancient civilizations, objects of iron from those days tend to be rare due to its tendency to oxidize and corrode. The objects that survived have been dated to be as much as 5000 years old. The Iron Age was from 1500 BC to 100 A. D, an era that was marked by almost constant war. In more peaceful times, magnetic iron was used in navigation, agriculture and architecture. Even today, 90% of all metal refined is iron-related and produced in the form of steel.

Iron Oxide

Iron oxide comes in multiple different forms, the common ones being hematite (α-Fe_2O_3), maghemite (γ-Fe_2O_3) and magnetite (Fe_3O_4). It is important to distinguish between the different forms as each has a unique magnetic moment, and interacts with an external magnetic field differently. Of the three forms that are mentioned above, hematite is the most stable, with maghemite and magnetite following with decreasing stability. As a result, a magnetite nanoparticle, if continuously exposed to air will oxidize into a maghemite nanoparticle. However, magnetite also has the bigger magnetic moment, which in medical applications can be advantageous[17].

In terms of structure, both maghemite and magnetite are spinels, with magnetite being an inverse spinel[18] and maghemite being a normal spinel. Both spinel oxide materials present with an XZ_2O_4 arrangement, but inverse spinels are slightly different and have the Z atoms distributed equally between the tetrahedral (A) and octahedral (B) sites (Figure 1). Consequently, Fe_3O_4 can also be written as $(Fe^{3+})_A(Fe^{3+}Fe^{2+})_BO^{2-}{}_4$, while γ-Fe_2O_3 is $(Fe^{3+})_A(Fe^{3+})_BO^{2-}{}_3$. Iron atoms in the tetrahedral sites are bonded to 4 oxygen atoms, whereas those in the octahedral sites are surrounded by 6 oxygen atoms[19].

Due to the similarities in structure between maghemite and magnetite, it is not easy to distinguish between the two different compounds with simple crystallographic analysis. A technique that can distinguish between the different valence states of Fe atoms, like Mössbauer Spectroscopy can help in that regard.

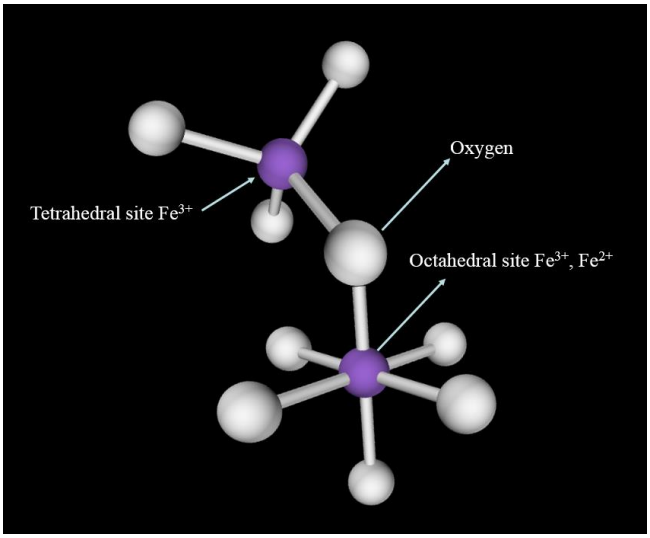


Figure 1 Magnetite tetrahedral and octahedral structure

Verwey Transition

For bulk magnetite, the resistivity in the material can increase dramatically below 119 K[20]. This Verwey transition is thought to result from a decrease in "electron hopping" between Fe^{2+} and Fe^{3+} in the octahedral sites[21]. At room temperature, it has been speculated that there is sufficient thermal energy to overcome the electron "hopping" energy barrier between the Fe^{2+} and Fe^{3+} ions. As the temperature decreases, this "hopping" becomes less likely, which increases the resistivity of magnetite below these temperatures. As a result of the electron hopping, some like to refer to room temperature magnetite as structurally being $(Fe^{3+})_A(2Fe^{2.5+})_BO_4$ instead of $(Fe^{3+})_A(Fe^{3+}Fe^{2+})_BO_4$.[22]

Stoichiometry

It is well known that the oxidation of magnetite to maghemite in bulk samples occurs as a result of the conversion of Fe^{2+} on the B-sites into Fe^{3+}. Specifically, to conserve the charge of the B-site, three Fe^{2+} converts to two Fe^{3+} and a vacancy (☐). To properly account for this oxidation, a more general chemical formula, which incorporates both maghemite and magnetite have to be used. Using x as the number of the Fe^{2+} ions converting to Fe^{3+}, and accounting for the creation of the vacancies (☐), the general formula is $(Fe^{3+})_A[(Fe^{2+})_{1-3x}(Fe^{3+})_{1+2x}\square_x]_BO_4$.[23] Alternatively, if the electron hopping is taken into account, $(Fe^{3+})_A[(Fe^{2.5+})_{2-6x}(Fe^{3+})_{5x}\square_x]_BO_4$ is the formulation.

To quantitatively evaluate the stoichiometry of a particular magnetite sample, we compare the $Fe^{2.5+}$ contributions to Fe^{3+} from both sites. This ratio $\frac{Fe^{3+}}{Fe^{2.5+}}$ can be written as:

$$\frac{Fe^{3+}}{Fe^{2.5+}} = \frac{1+5x}{2-6x} \tag{1}$$

This equation is only valid above the Verwey transition, since below that, the electron hopping ceases. From equation (1), when x = 0, as is the case where no oxidation has occurred, $\frac{Fe^{3+}}{Fe^{2.5+}}$ is 0.5. The larger x, the larger the amount of oxidation.

For cases where the experiment is performed below the Verwey transition, the configuration $(Fe^{3+})_A[(Fe^{2+})_{1-3x}(Fe^{3+})_{1+2x}\square_x]_BO_4$ is more appropriate, so the ratio $\frac{Fe^{3+}}{Fe^{2+}}$ becomes:

$$\frac{Fe^{3+}}{Fe^{2+}} = \frac{2+2x}{1-3x} \tag{2}$$

From equation (2), when x = 0, as is the case where no oxidation has occurred, $\frac{Fe^{3+}}{Fe^{2+}}$ is 2.

Magnetism

Magnetism exhibited in iron compounds includes, ferromagnetism, ferrimagnetism antiferromagnetism and paramagnetism.

Magnetic moments are generated from the intrinsic spin and orbital of the electrons. In a material, electrons are typically paired up according to Hund's rules and Pauli's exclusion principle. As a result the material will tend to show a net zero magnetic moment, since the opposing moments in paired electrons will cancel each other out. However, in atoms that contain partially filled shells, there is the possibility for a net magnetic moment to exist. In a paramagnetic material, the unpaired electrons will align in an external magnetic field. However, once the external field is removed, the unpaired electrons will return to their original state, with the net magnetic field outside the material returning to zero (Figure 2). This is because in a paramagnet, thermal motion inside the material is enough to randomize the magnetic moments without the presence of an external field. For a ferromagnet and ferrimagnet, the individual magnetic moments in a magnetic material will typically organize themselves into several magnetic domains within the material, with each domain containing a number of magnetic moments that are aligned with each other.

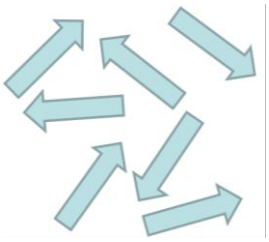


Figure 2 Magnetic moments in a paramagnet.

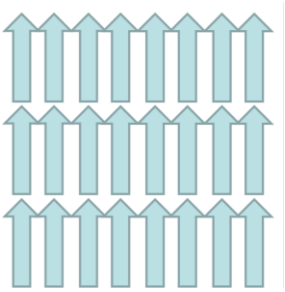


Figure 3 Magnetic moments in a ferromagnet.

A ferromagnet is a material that will have its magnetic domains aligned in an external magnetic field. In addition, a ferromagnet will partially retain this alignment after removal of the external field, becoming a permanent magnet. More specifically, a ferromagnet will have its magnetic moments aligned in the same direction of an applied magnetic field (Figure 3). Elemental iron is a ferromagnet.

Ferrimagnets like ferromagnets, have net positive magnetic moments in an applied external field. Similarly, ferrimagnets will retain their magnetization after removal of the magnetic field. However, the difference between the two is that ferrimagnets have net magnetic moments that are decreased by opposing magnetic moments in different crystallographic sites within the ferrimagnet itself (Figure 4).

Ferrimagnetism is also what bulk magnetite and maghemite exhibit. An antiferromagnet is similar to a ferrimagnet in that neighboring crystallographic sites carry opposing electrons that generate opposing magnetic moments, however in this case, the moments are equal in magnitude (Figure 5). As a result, the net magnetic moment of an antiferromagnet is zero, and the material is not attracted by an external field. (Figure 4).

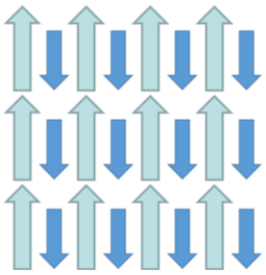


Figure 4 Magnetic moments in a ferrimagnet.

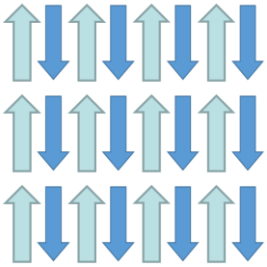


Figure 5 Magnetic moments in antiferromagnet.

Curie Temperature

When heat is applied to a ferromagnet, ferrimagnet or antiferromagnet, there is increased randomization of the magnetic moments within them. If the temperature is increased beyond a certain threshold, the thermal motion of these moments can become so severe as to render all three into a paramagnetic state. When this occurs, all the magnetic moments will be randomized once the external magnetic field is removed. This threshold is called the Curie temperature. Different compounds will have different Curie temperatures, for example, the Curie temperature of Fe_3O_4 is 858 K, while it is γ-Fe_2O_3 is 948 K[24]. Generally, the higher the temperature, the bigger the magnetic field needed to generate magnetization in a paramagnet. A similar transition exists in antiferromagnets, called the Néel temperature.

Larmor Precession

In the presence of a magnetic field, magnetic moments will precess or rotate around the axis of magnetization. This movement is called the Larmor Precession. If the moments are not fully aligned with the field, which tends to happen at room temperatures, there will be an angle of precession. (Figure 6).

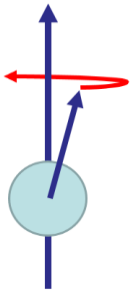


Figure 6 A magnetic moment precessing around a magnetic field.

Superparamagnetism

Ferromagnets and ferrimagnets of sufficiently small size have magnetic moments that flip randomly under the influence of temperature. Such ferrimagnets and ferromagnets are usually in nanoparticle form and the random flips present a net zero magnetization outside an external magnetic field. Inside an external field, the magnetic moments will align to the external field. That behavior is similar to that of a paramagnet. Materials that are ferromagnetic and ferrimagnetic in bulk form, but present as a paramagnet below their Curie temperature are referred to as superparamagnets.

Magnetic Anisotropy

The easy axis is the preferential direction where the magnetic moments will align without an external magnetic field. To move the magnetic moments from the easy axis, energy will have to be applied to the moments, typically using an external magnetic field or increasing the temperature. The energy is related to the magnetic anisotropy[25], *K*, by the equation:

$$E = KVsin\theta \quad (3)$$

Magnetic anisotropy is characteristic of individual materials. equation (3) shows that the smaller the domain size, the lower the energy barrier needed to move the magnetic moments away from the easy axis. As a result, even ambient temperature can provide enough thermal energy for the moments to flip, resulting in superparamagnetism.

The positions that the magnetic moments 'flip' between are antiparallel to each other. The time spent travelling between the two positions is typically referred to as the 'relaxation' of the magnetic moments and the relaxation occurs according to Néel's theory of superparamagnetism[26]. Each

individual sample also has a characteristic relaxation time of τ_0, and relates to the relaxation time (τ) and magnetic anisotropy (K) by:

$$\tau = \tau_0 \, exp\left(\frac{KV}{kT}\right) \tag{4}$$

Blocking Temperature

Since the flipping of the magnetic moments in superparamagnets is a result of thermal motion, it follows that removal of heat can facilitate the appearance of spontaneous magnetization in the particles. The temperature where this occurs is called the blocking temperature. This can be expressed as equation (5), which states the relationship between the measurement lifetime (τ_m) and the characteristic relaxation lifetime (τ_0).

$$T_B = \frac{aKV}{k} \tag{5}$$

where, $a = 1/ln(\tau_m/\tau_0)$. To appropriately measure these superparamagnets, a measurement technique which has a measuring time shorter than that of the relaxation time is needed. In Mössbauer spectroscopy, the measuring time is about 10^{-9} s, which is close to the typical relaxation time of the SPIONs of around 10^{-10} s.[27] The difference in the measuring time and the relaxation time can be met by increasing the relaxation time of the SPIONs. This can be achieved by cooling the SPIONs.

Mössbauer Spectroscopy

The Mössbauer Effect was discovered by Rudolf Mössbauer[28]. Previously, it had been observed that optical resonance can be achieved from excited gases. However, gamma-ray resonances had not been observed to be producible through gas excitation. Since the recoiling of atoms in gases was unavoidable after emission, resonance was not likely. Some of the gamma ray energy that is emitted is lost to recoil, and this energy is not sufficient to excite the nuclear transitions and thus resonance could not be achieved.

In experiments involving iron compounds, the source is ^{57}Co, which decays to ^{57}Fe and emits gamma rays. Gamma rays with energy of 14.4 keV (E) are particularly useful for iron related experiments. The recoil energy, (E_{recoil}), can be calculated for a ^{57}Co source, which is unbounded:

$$E_{recoil} = \frac{E^2}{2mc^2} \approx 0.002eV \tag{6}$$

The important point here is that the recoil energy is 0.002 eV. However, the linewidth of a typical Mössbauer spectrum is much smaller, usually in the 10^{-9} eV range. As a result this recoil energy has to be accounted for to resolve the linewidths and for resonance to be achieved.

To create a gamma ray resonance system, the emitted gamma ray used needs to have energy that matches the nuclear transition energy and compensates for the recoil energy (0.002 eV). If one were to allow both absorber and emitted nuclei to be bound within a solid lattice, the mass (m) term in the equation (6) would be the mass of the whole lattice. Recoil energy will be minimal as a result. Consequently, it can be understood that the reason resonance is impossible to achieve in gases is because there are no recoilless atoms. This fraction is now understood to be the Mössbauer-Lamb fraction (f), where θ_d, is the Debye temperature of the material.

$$f = exp\left(-\frac{E_{Recoil}}{k{\theta_d}^2}\left(\frac{3}{2} + \frac{\pi^2 T^2}{{\theta_d}^2}\right)\right) \tag{7}$$

To modulate through the energies required to produce resonance in a particular sample, the radioactive source is Doppler shifted by being vibrated. This is typically in the range of mm/s.

Three important quantities in the Mössbauer experiment are described; the isomer shift (IS), the magnetic hyperfine field (HF) and the electric quadrupole splitting (QS). These three quantities are unique for different materials and compounds and are used to determine the structure, magnetism and stoichiometry of a material where Mössbauer resonance can be achieved.

Low Temperature Experiments

As can be seen from the Mössbauer-Lamb fraction equation, a decrease in temperature in Mössbauer spectroscopy experiments corresponds to an increase in the fraction, which in turn contributes to an increase in the signal-to-noise ratio of the spectrum. Furthermore, a sub-room temperature experiment is required to properly resolve the spectra where there is a blocking temperature, as is the case for a superparamagnetic material.

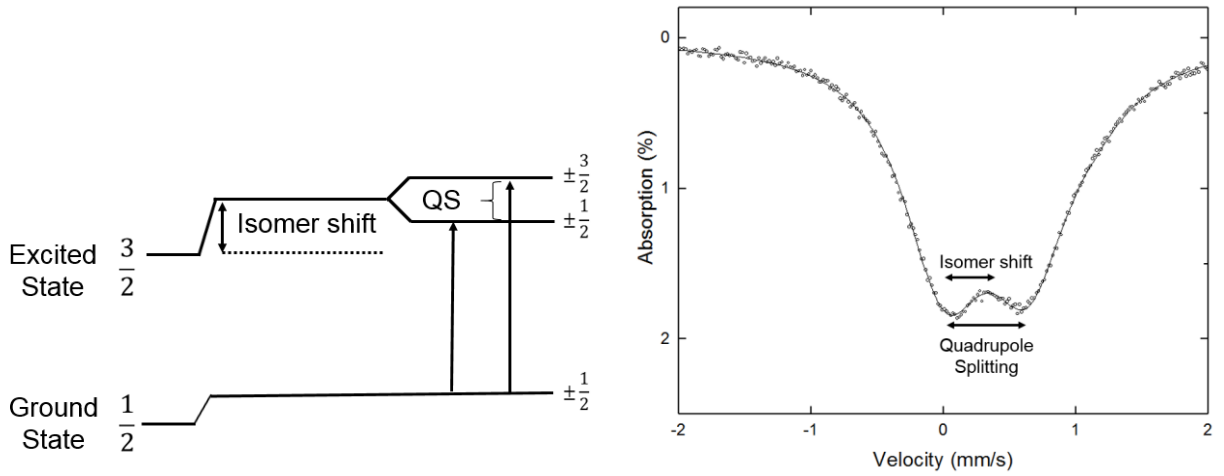


Figure 7 The nuclear transitions of the sample; the difference between the energies in the excited states of the source and the sample results in the isomer shift. The spectrum presented is of a superparamagnetic sample of maghemite at room temperature.

Isomer Shift

The s-electrons of an atom has some probability of existing within the nucleus. As a result, there is electrostatic energy generated by this interaction, commonly referred to as the electric monopole interaction. For different compounds, the electron density around and inside the nucleus is characteristic of that compound and the strength of the electric monopole interactions differ from compound to compound. An isomer shift is therefore generated when the compound is compared to the reference material, commonly α-Fe for iron Mössbauer experiments. This is because α-Fe has differing energy levels when compared to a compound that carries different electron densities around its nucleus (Figure 7). Second order Doppler shifting (SODS) can also contribute to the additional shifting. A relativistic effect, SODS tend to be so minute at room temperature as to be negligible. At temperatures where the Debye temperature is much larger than the experiment temperature, the SODS becomes more prominent. For α-Fe, that means an increase of about 0.1 mm/s at 5 K.

Quadrupole Splitting

A quadrupole splitting can be found in compounds that have an asymmetrical charge distribution resulting from the electrons surrounding the nucleus. An asymmetrical charge distribution creates an electric gradient around the nucleus and the interaction between the nucleus and the gradient gives QS.

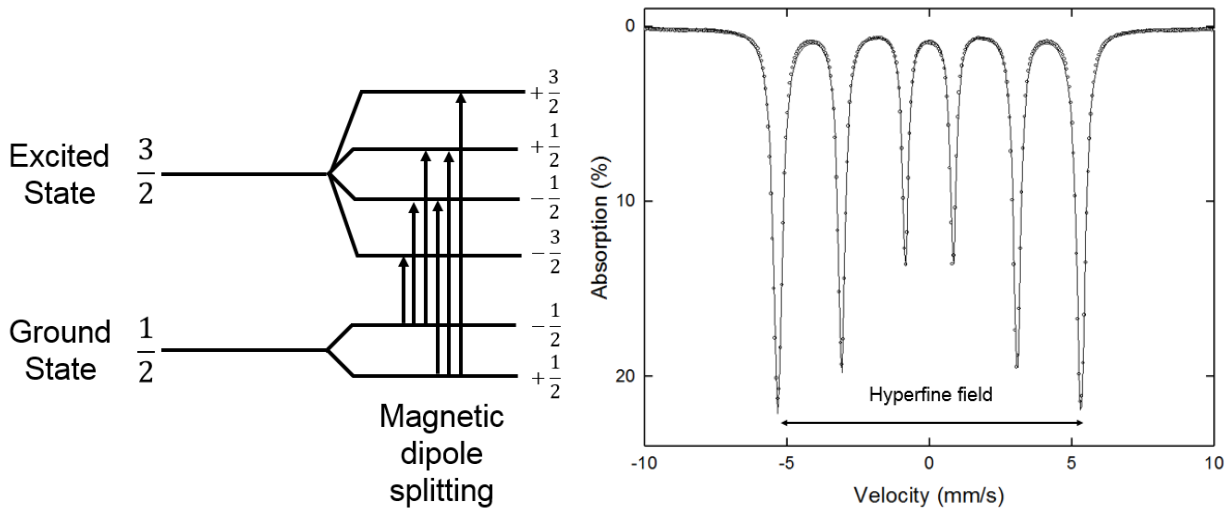


Figure 8 The effect of magnetic dipole splitting on the energy levels; each transition corresponds to a peak in the spectrum. The spectrum obtained is a-Fe at room temperature.

A nucleus with a flattened shape will present a QS of negative magnitude whereas an elongated nucleus will have a positive QS (Figure 7).

Magnetic Hyperfine Field

The magnetic field generated at the nucleus by interaction with the electrons gives a magnetic hyperfine field that can be observed by Mössbauer spectroscopy.

This hyperfine field, is characteristic for each compound as the configuration of the electrons in the crystals around the nucleus largely determines the strength and direction of the field. In α-Fe, the hyperfine field is about 330 kG at room temperature (Figure 8) whereas for some oxides, it could be as large as 500 kG.

Since there is a magnetic moment at the nucleus, an applied external magnetic field can interact with it, and depending on the direction of the field, can either increase or decrease the observed hyperfine field. These experiments are valuable since some samples contain multiple compounds and applying a magnetic field to separate the hyperfine fields is one method to distinguish materials or sites.

Linewidth

Understanding that the uncertainty principle explains that given a photon of some lifetime, there will be some uncertainty associated with its energy, an equation for the natural linewidth, Γ, of a Mössbauer spectrum can be found by:

$$\Gamma = \frac{\hbar}{t} \tag{8}$$

The 14.4 keV gamma ray emitted by the radioactive source ^{57}Co used in iron-related Mössbauer spectroscopy has an excited lifetime, t, of 10^{-7} s, and as mentioned earlier is in the 10^{-9} eV range. From the above equation, the natural linewidth is found to be about 0.22 mm/s. Typically in an experiment, the linewidth is slightly broader due to the instrument.

Motional Narrowing

In Nuclear Magnetic Resonance, motional narrowing refers to the narrowing of linewidths as the temperature is increased[29]. This phenomenon can be extended to Mössbauer spectroscopy by observing that the linewidths narrow as temperature is increased. While not commonly used in Mössbauer spectroscopy, the relation between the change in the linewidth, $\Delta\Gamma$, and the relaxation time of the sample can be expressed by the equation,

$$\Delta\Gamma = \omega^2\tau \tag{9}$$

The relaxation time, τ, is temperature dependent and each sample has a characteristic relaxation time, τ_0. These parameters relate to the blocking temperature as described by equation (5). The ω here is the hyperfine field converted to angular frequency, and is the instantaneous hyperfine field "seen" by the relaxing magnetic moments, assuming it can be measured. It is because this instantaneous field cannot be measured instantaneously without manipulation that the lines are narrow, since only the average field is observed. When the relaxation time is reduced by cooling the sample, slowing down relaxing moments, the average field "seen" increases, and the lines broaden.

Chapter 2 Experimental Methods

Synthesis of Iron Oxide Nanoparticles

The samples of iron oxide nanoparticles that are used here come from Xavier University in Louisiana. The synthesis is described in detail by Goloverda et al[30]. Using $FeCl_2$, $FeCl_3$ and diethylene glycol as the raw materials, the synthesis follows the chemical equation:

$$[Fe(DEG)Cl_2]^{2-} + 2[Fe(DEG)Cl_3]^{2-} + 2H_2O + 2OH^- \rightarrow Fe_3O_4 + 3H_2DEG + 8Cl^-$$

The size of the iron oxide nanoparticles was controlled by increased initial reaction temperature as well as reaction time. The reactions were done in a controlled nitrogen atmosphere, utilizing a Schlenk line. The sizes of the nanoparticles are 5.3 nm, 8.6 nm, 10.6 nm and 11.9 nm.

Characterization

Methods of characterization include Dynamic Light Scattering (DLS), Transmission Electron Microscopy (TEM), and X-ray diffraction (XRD) as well as Mössbauer spectroscopy.

TEM

TEM images of the nanoparticles were obtained to determine the size of nanoparticles that were produced (Figure 9).

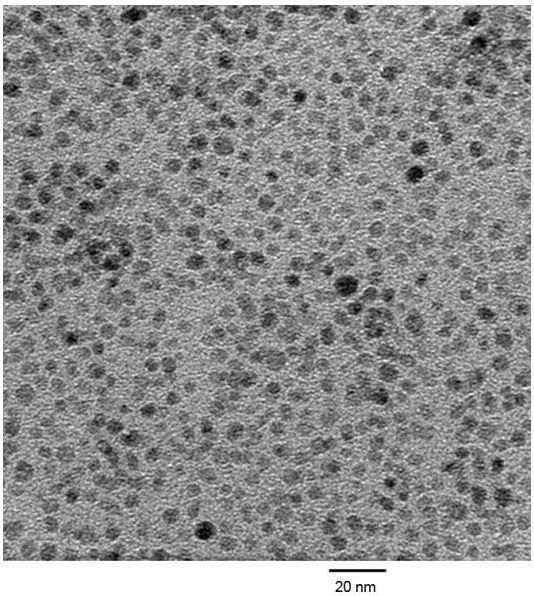


Figure 9 TEM of 5.3 nm iron oxide nanoparticles.

XRD

X-ray diffraction data allowed for a confirmation that either magnetite or maghemite was formed during the reaction, although not providing a distinction between the two. Furthermore, using the Scherrer's equation, which despite its flaws allowed for an approximation of the size of the nanoparticles, corroborate the data found with TEM.

Mössbauer Spectroscopy

The Source

^{57}Fe makes up about 2% of naturally occurring iron, with the majority of iron being ^{56}Fe. As a result, decay of ^{57}Co (half-life of 270 days) through electron capture to the I =5/2 ground state of ^{57}Fe can produce the gamma rays of appropriate energy to match the transitions of an iron atom. Since the ^{57}Fe itself is magnetic and has its own Zeeman splitting which can complicate the Mössbauer spectrum, the source ^{57}Co is diffused into a rhodium matrix to quench the splitting.

Additionally, the source is vibrated by a Mössbauer Drive (Figure 10), to achieve the required transitions. Typically, the vibrations were performed in either ranges of ±12 mm/s for magnetically split spectra and smaller ranges for doublets or singlets.

The Detector

^{57}Fe Mössbauer spectroscopy uses a proportional counter filled with krypton gas, with a small amount of methane used as the quench gas.

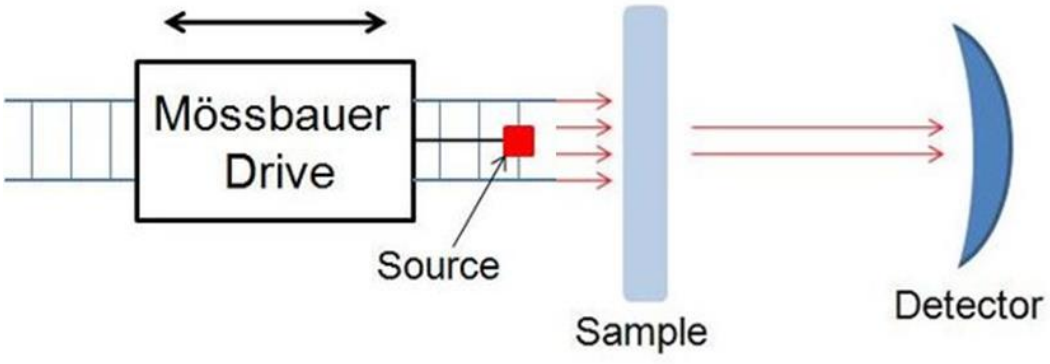


Figure 10 A Mössbauer experimental setup.

The working principal of the counter is that incident 14.4 keV resonant gamma-rays received from the sample interacts with the krypton gas and generates a peak in the pulse height spectrum when the ionized krypton reaches the electrode. However, a portion of the 14.4 keV gamma ray generates x-rays which 'escape' the detector, but about 2 keV of those 14.4 keV gamma rays do interact and generate another peak (Figure 11).

The first peak in the pulse height spectrum is electronic noise, the second peak is the 2 keV escape peak which has Mössbauer information; the third peak is from x-rays generated from the iron in the sample; the fourth peak is the 14.4 keV Mössbauer peak from the source and sample; the last peak is x-rays resulting from the rhodium matrix. The peaks that carry the resonance information are selected for counting.

The Sample

The iron oxide nanoparticles from Xavier University were stored in a glovebox. To ensure that the iron oxide nanoparticles do not oxidize further when transitioning between the glovebox and Mössbauer setup, the samples were transported in a nitrogen filled dewar. The samples were then prepared by sticking them to the round side of a sample holder (Figure 12), using vacuum grease as the adhesive.

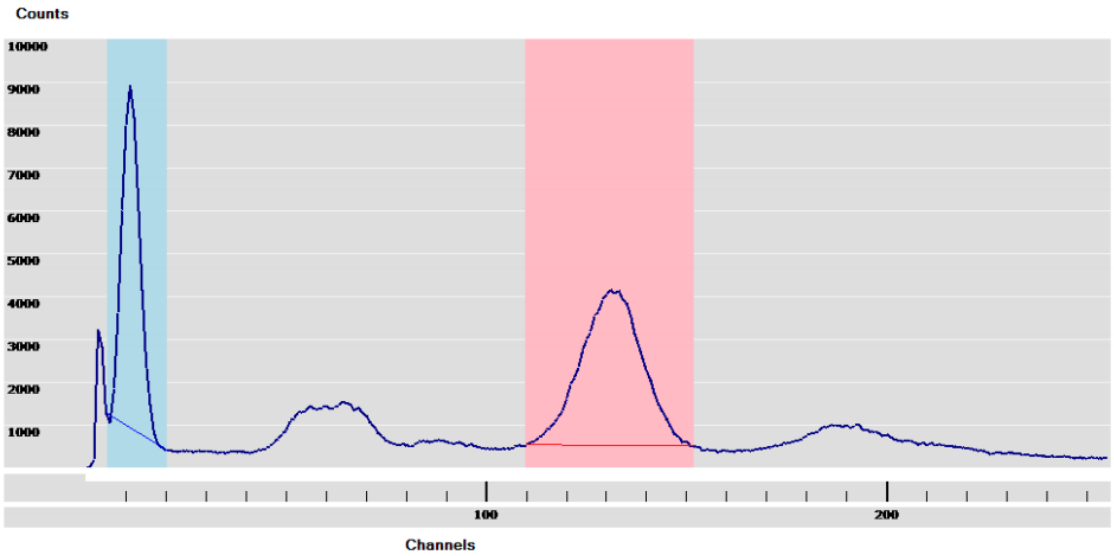


Figure 11 The pulse height spectrum on the Mössbauer detector. The red and blue boxes show the peaks selected for counting.

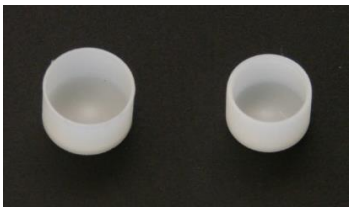


Figure 12 Sample holder for the iron oxide nanoparticles.

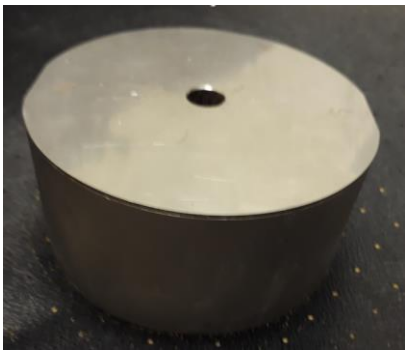


Figure 13 The 20 kG magnet, the sample is placed in the hole during experiments.

By spreading the sample to the round side of the sample holders and aligning that side to the source, the gamma-rays are exposed to the largest cross section of the samples, generating the highest amount of interaction between the gamma rays and the samples.

Experiments in External Magnetic Field

For experiments done in a magnetic field, Nd-Fe-B permanent magnets were used, with the field strengths being 3.8 kG, 10 kG and 20 kG. For the magnets of 10 kG and 20 kG the configuration of the magnets were in a Halbach dipole arrangement (Figure 13). The magnetic fields were either in a parallel or perpendicular alignment to the gamma-rays when the experiments were performed.

Low Temperature Experiments

Low temperatures were achieved by using a cryogen-free cryostat, with the sample being mounted into the cryostat with a metal rod. This cryostat, a Janis SHI-850-5 (Figure 14), operates according to the Gifford-McMahon Refrigeration cycle.

The temperatures range between 4.2 K to 325 K. A semi-conductor at the sample space measures the temperature of the sample, whereas a heater in the rod is used to increase temperature. The sample space is filled with helium gas to provide good thermal conductivity between the cold head and the sample.

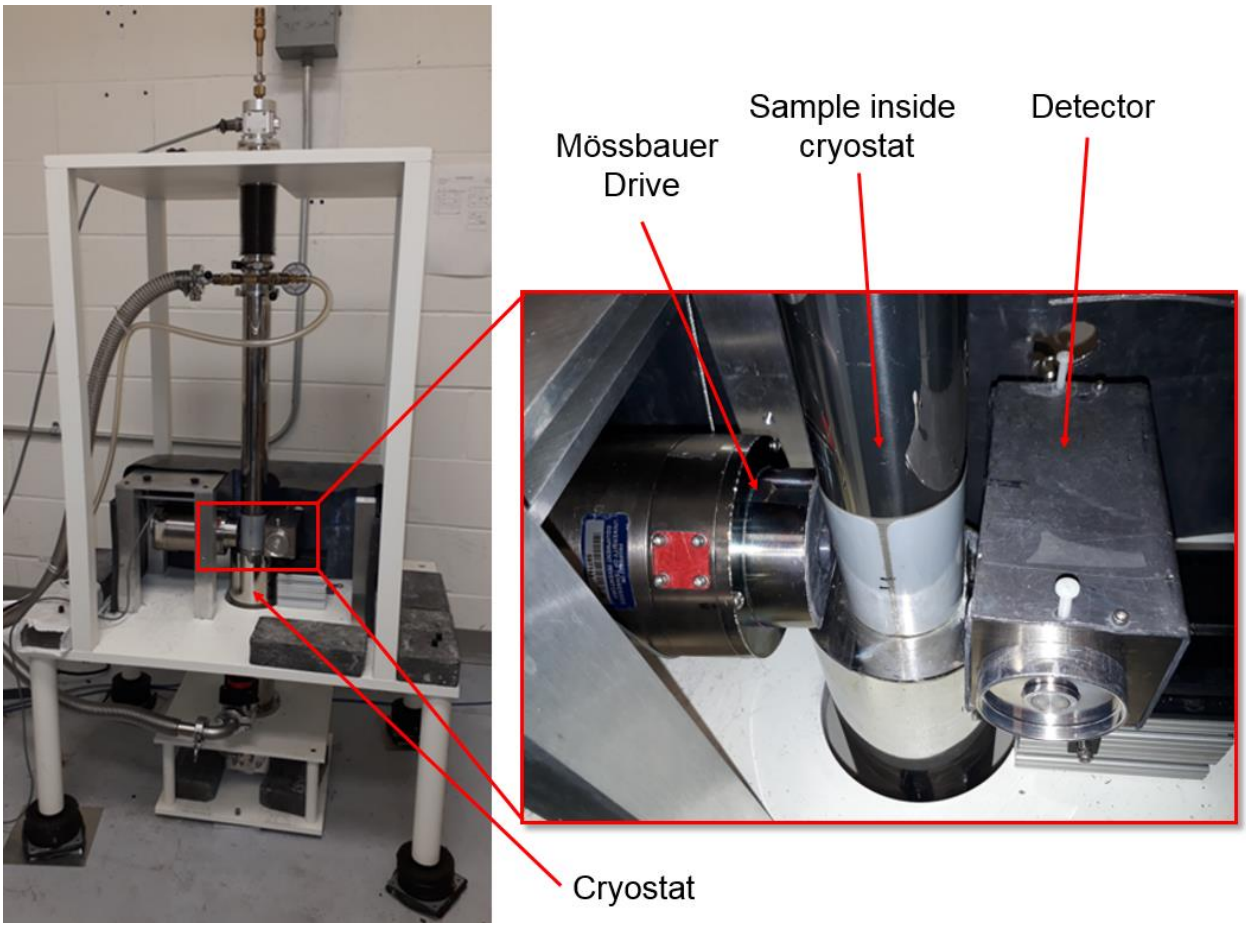


Figure 14 The cryostat with the Mössbauer setup.

Vibrations from the cryostat during operation can broaden the linewidth of the Mössbauer spectra. Considering that motional narrowing analysis requires measurement of the linewidths, the vibrations need to be minimized. For that reason, the cryostat is mounted onto a set of bellows at each foot. Furthermore, the Mössbauer drive is suspended from wires to minimize contact with the cryostat frame. Every few months, the cryostat was realigned to ensure optimal geometry for experiments while also minimizing the vibrations.

Fitting Methods

The spectra obtained were fitted using the Mössbauer Data Analysis Program provided by Robert S. Preston (Northern Illinois University) and Dennis E. Brown. This program is mainly utilized for Lorentzian fitting. For motional narrowing, where a Voigt function is needed, Origin is used. Ultimately, the programs can give the values for the hyperfine field, isomer shift, quadrupole splitting, line intensities, spectral areas and linewidths.

Chapter 3 Results and Discussion

Mössbauer spectroscopy: Bulk magnetite and maghemite

Once the initial magnetite measurements were performed, the samples were kept in the glovebox. However, when the samples were revisited about three years later, some interesting discrepancies were found between the initial and newer measurements, oxidation of the nanoparticles from magnetite to maghemite was the probable cause[31,32].

Simply because the details of both bulk magnetite and maghemite will be referred to in this discussion, it is appropriate to do an analysis of these materials for comparison. At room temperature, the two have very different Mössbauer spectra, with magnetite having two distinct crystallographic sites, tetrahedral (red) and octahedral (green), and a hyperfine field of 490 kG for the tetrahedral site and 460 kG for the octahedral site (Figure 15). For maghemite, the two sites are less distinct and the octahedral site has a hyperfine field of 502 kG. On the tetrahedral site, the hyperfine field is 490 kG[33]. The results are in good agreement with other studies. The important thing to note here is that at room temperature for bulk materials, the two materials are qualitatively distinguishable by Mössbauer spectroscopy.

Stoichiometry: Qualitative and Quantitative Analysis

Analysis of the stoichiometry of the samples can be both qualitative and quantitative. The simplest form of qualitative analysis for these samples is by eye. Since magnetite and maghemite are different colors, one can easily observe that if the samples are predominantly either maghemite or magnetite (Figure 16). Maghemite is a brownish color, whereas magnetite is closer to black. However, the question of how oxidized, or in other words, how stoichiometric the samples are, cannot easily be determined visually, especially if the sample is a mixture of both magnetite and maghemite. One method would be to obtain Mössbauer spectra of the samples at room temperature and find whether there are distinct tetrahedral and octahedral sites as shown in Figure 15.

The question of how stoichiometric our samples are has to be decided by different methods. There are several potential methods, but all methods used here revolve around comparing the stoichiometry of the sample to general nonstoichiometric chemical formulae of magnetite, one being $(Fe^{3+})_A[(Fe^{2+})_{1-3x}(Fe^{3+})_{1+2x}\square_x]_BO_4$. To do this, the spectroscopic areas of the A and B sites (from Figure 15) can be used in conjunction with equation (2).

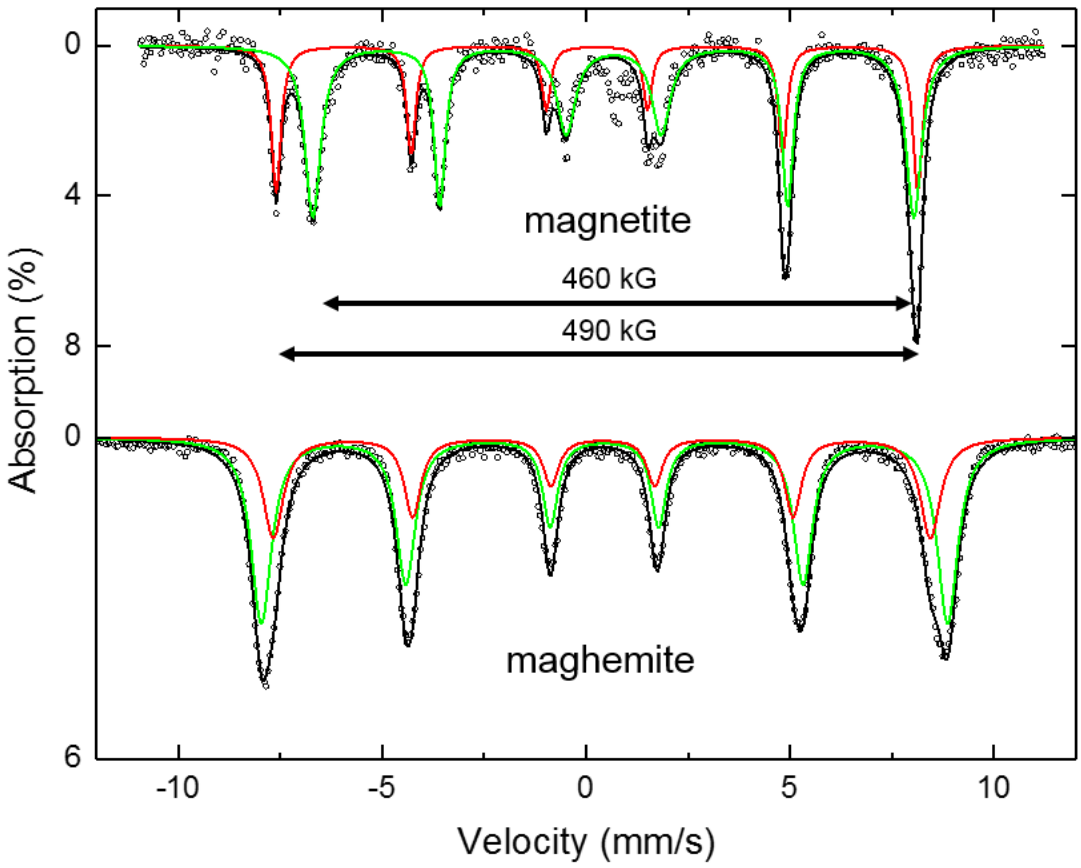


Figure 15 Bulk magnetite and maghemite at room temperature. The red lines are the tetrahedral sites, with green representing the octahedral sites.



Figure 16 Bulk forms of magnetite and maghemite.

However, for nanoparticles below a certain size, these A and B sites are less resolved. For example, a plot of high temperature spectra of magnetite nanoparticles show no distinct hyperfine fields for the nanoparticles 5.3 nm, 8.6 nm and 10.6 nm (Figure 17 and Figure 18). Qualitatively, Figures 17 and 18 show that the samples 8.6 nm and 5.3 nm have oxidized into maghemite over the three-year period. The magnetite samples in Figure 17 show an asymmetrical singlet, whereas the maghemite samples in Figure 18 present as doublets. The 11.9 nm sample seems to have remained the same and the 10.6 nm linewidth has broadened slightly, from 2.5 mms^{-1} to 3.0 mms^{-1}, when fitted as a singlet. The 10.6 nm therefore has some ambiguity and a more detailed stoichiometric analysis has to be done. The task is to extract the distinct crystallographic sites in the analysis for the 5.3 nm, 8.6 nm and 10.6 nm nanoparticles. Two methods are used here, one is by cooling the samples to below the blocking temperature, and the other is to apply a magnetic field. Both methods are utilized to 'block' the relaxation in the particles.

Since both magnetite and maghemite are ferrimagnets with octahedral and tetrahedral sites pointing in opposite directions, applying a magnetic field will increase the hyperfine field of one site and decrease it for the other, causing the two sites to separate. More specifically, since the hyperfine field lies in the opposite direction of the magnetic moment and the larger magnetic moment will align with the magnetic field, the octahedral site, which has two iron atoms will align with the magnetic field. Its hyperfine field will therefore decrease while the hyperfine field on the tetrahedral site will increase.

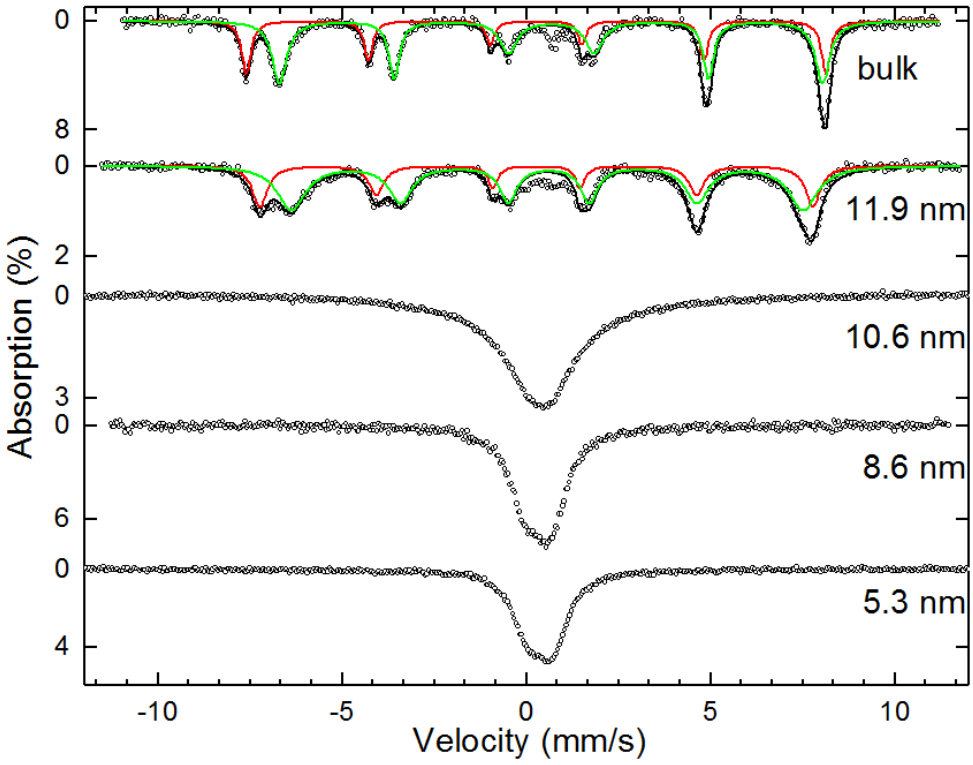


Figure 17 Mössbauer spectra of iron oxide nanoparticles, magnetite nanoparticles at room temperature.

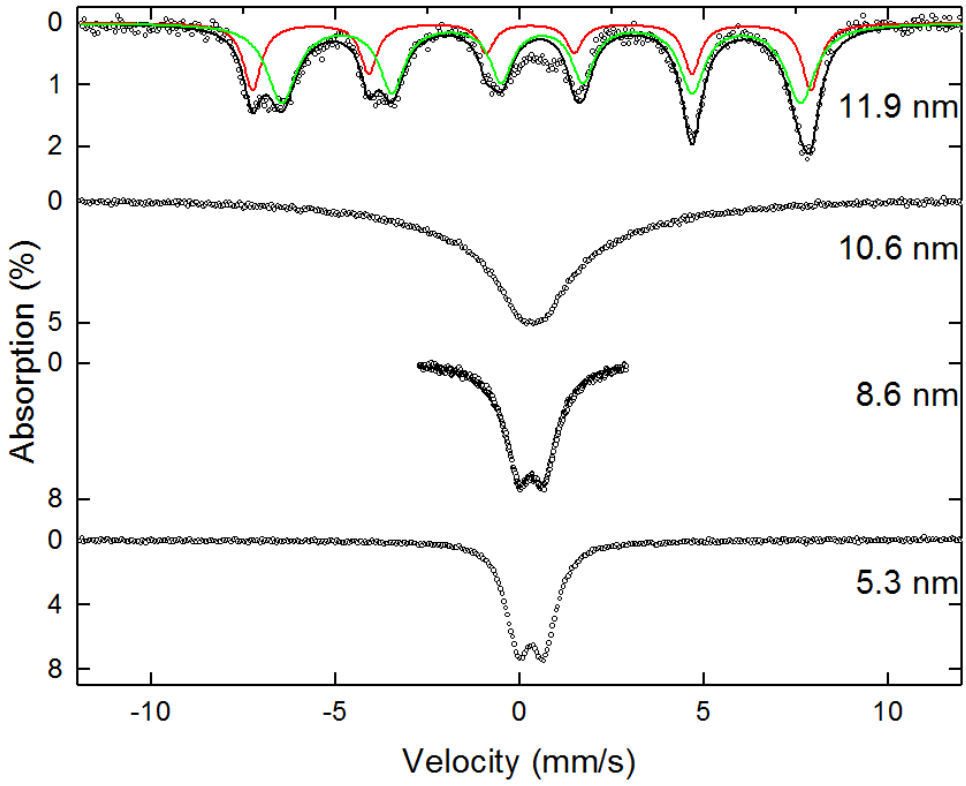


Figure 18 Mössbauer spectra of maghemite nanoparticles, at room temperature.

Low Temperature Experiments

Low temperature experiments, performed at 6 K, were previously presented in the Master's thesis. In summary, the Fe^{2+} shown in Figure 19 proves that the samples are mostly magnetite, and the spectra are fitted similar to Berry *et al*[34], with two Fe^{3+} (one on the tetrahedral and octahedral site) and two Fe^{2+} sites (both on the octahedral site). However, when compared to the same experiments on the maghemite samples, the Fe^{2+} at the octahedral site for the 5.3 nm, 8.6 nm and 10.6 nm has mostly disappeared, becoming maghemite (Figure 20). Furthermore, the complicated sub-spectra of the tetrahedral site for the samples 5.3 nm, 8.6 nm and 10.6 nm is gone and replaced by one Fe^{3+} site. Since only the Fe^{3+} lines are left and have similar parameters (Table 1), the oxidized octahedral and tetrahedral sites overlap heavily, just like maghemite. This is consistent with the oxidation of magnetite to maghemite. The 11.9 nm nanoparticle is mostly unchanged from the initial experiments.

The 5.3 nm sample appears to be completely oxidized, since it presents like maghemite. However, the 8.6 nm and 10.6 nm samples show small amounts of Fe^{2+} after oxidation, which can be understood to be a result of having smaller surface area to volume ratios than the 5.3 nm, and hence oxidizing at a slower rate. The increased broadness of the 10.6 nm line between the maghemite and initial magnetite samples at room temperature can be explained by the maghemite sample being a doublet (or in other words like two overlapping singlets) but due to the broadness of the lines, the quadrupole splitting is not visible.

The magnetite nanoparticles are fitted with the hyperfine parameters listed in Table 1. All the spectra shown in Figure 19 have been fitted with the same hyperfine parameters. This is justified by the fact that the largest hyperfine field of a material occurs at 0 K and is of the same magnitude regardless of particle size. Note that there are two Fe^{2+} sites, distinguished by their larger isomer shifts (IS).

While this sounds like a contradiction to what was stated previously, some have speculated that this is a result of the structural change that occurs below the Verwey transition[35]. This is supported by the fact that electron-hopping has ceased at these temperatures.

Fitting with the same parameters was not possible for the maghemite samples, since the Fe^{3+}/Fe^{2+} combination as well as the structure is different.

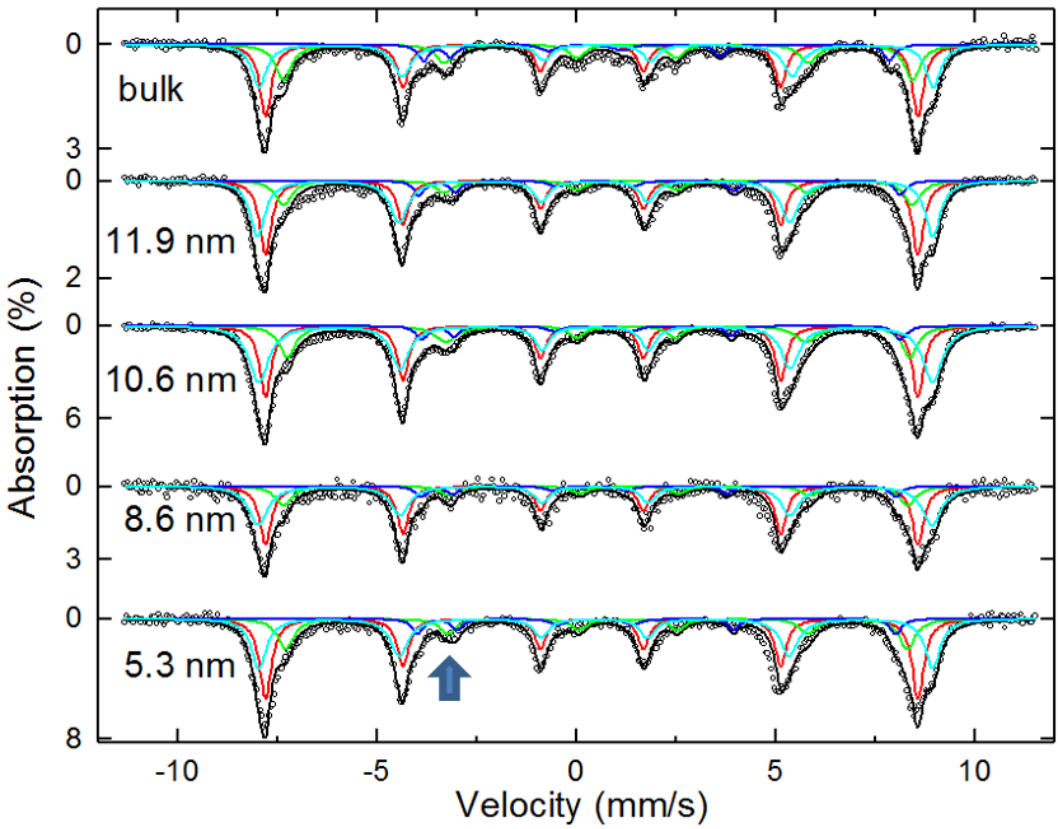


Figure 19 Mössbauer spectra of magnetite nanoparticles, initial experiments at 6 K. The arrow is pointing to the Fe^{2+} on the octahedral site, fitted with a blue line. The red line represents the tetrahedral sites while the rest are sub-spectra of the tetrahedral site.

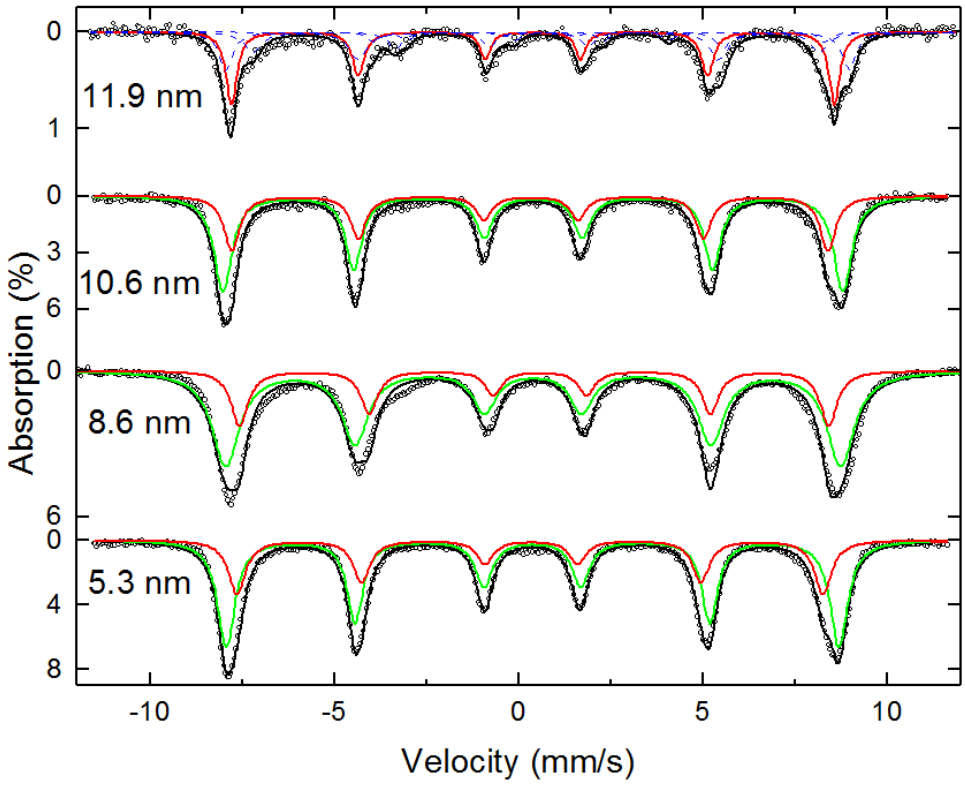


Figure 20 Mössbauer spectra of maghemite nanoparticles, at 6 K, the blue dash lines represent the sub-spectra at the tetrahedral site. The 5.3 nm, 8.6 nm and 10.9 nm nanoparticles have oxidized.

Table 1 Low temperature hyperfine parameters.

Site	**B_{hf} (kG)**	**IS(mm/s)**	**QS(mm/s)**
A(Fe^{3+})	507	0.41	0
B(Fe^{3+})	524	0.5	0
B(Fe^{2+}i)	489	0.91	-0.71
B(Fe^{2+}ii)	362	1.26	1.62

Low Temperature Experiments: Stoichiometry

The fits in Figure 19 and 20 allow for the determination of the population of each valence of iron atoms in the iron oxide samples, listed in Table 2. The x here refers to the one used in equation (2), and gives an idea of how stoichiometric the sample is. The "unoxidized" initial magnetite samples do have some oxidation, with the 5.3 nm sample having the smallest amount of oxidation at x = 0.07, and the 8.6 nm sample having the largest amount of oxidation and is most non-stoichiometric, with x = 0.12. The 11.9 nm sample which appeared to be unoxidized, due to its similarity to the bulk sample, when inspected visually on the Mössbauer spectrum is in fact slightly oxidized. What this also confirms is that while qualitative analysis can be valuable, the test is to determine the stoichiometry through quantitative analysis. Furthermore, although the same analysis cannot be done on the 5.3 nm, 8.6 nm and 10.6 nm samples due to being overwhelmingly oxidized and missing the Fe^{2+} sites, analysis of the 11.9 nm sample after 3 years shows x = 0.09. This shows that the 11.9 nm sample is remarkably stable, since increased oxidation for this sample caused the difference in x after three years to be only 0.01. Given that the bulk also shows x = 0.01, this could be an experimental or computational error, since a 100% stoichiometric bulk sample should be x = 0. To conclude, none of the nanoparticles are fully stoichiometric magnetite during the initial run of experiments, but have small amounts maghemite.

Table 2 Low temperature percentages of iron species of initial samples.

Particle size (nm)	**A(Fe^{3+})**	**B(Fe^{3+})**	**B(Fe^{2+}i)**	**B(Fe^{2+}ii)**	**Fe^{3+}/Fe^{2+}**	**x**
Bulk	36	32	23	9	2.1	0.01
11.9 nm	36	40	16	8	3.2	0.10
11.9 nm (after 3 years)	36	40	17	8	3.0	0.09
10.6 nm	34	41	19	6	3.0	0.09
8.6 nm	39	39	15	7	3.5	0.12
5.3 nm	38	35	19	8	2.7	0.07

Room Temperature Experiments: Stoichiometry

The room temperature experiments for the superparamagnetic nanoparticles (i.e. the 5.3 nm, 8.6 nm and 10.6 nm) are usually not considered for stoichiometric purposes due to not having distinct hyperfine fields[36]. However, the initial pre-oxidation magnetite experiments show a slightly asymmetric singlet, which seems to indicate some sort of structure (Figure 18).

Here an uncommon method of fitting high temperature Mössbauer spectra is explored. In the literature, it is found that some cases of magnetite above the Curie temperature of 858 K was fitted in this manner[37]. However, this model is not typically applied for magnetite spectra that have a blocking temperature below room temperature.

While the experiments here are below the Curie temperature, the blocking temperature is spectroscopically analogous to the Curie temperature for magnetite, so the fitting performed seems to be reasonable. (i.e. transitioning through the Curie temperature, a material goes from singlet/doublet to magnetically split; this also occurs as the experiments are recorded through the blocking temperature.)

Proceeding with fitting the asymmetric singlets and assuming them to represent the tetrahedral and octahedral sites give the results indicated in Table 3 and Figure 21.

The x-values obtained in Table 3 are a result of using equation (1), and is derived from understanding that above the Verwey transition, the iron at the octrahedral site is $Fe^{2.5+}$. If such a method were valid, the results would give mostly stoichiometric magnetite and x at low temperature would be equivalent to x obtained at room temperature.

Table 3 Room temperature percentages of iron species of initial samples.

	B_{hf} (kG)	**Fe^{3+}(%)**	**$Fe^{2.5+}$(%)**	**$Fe^{3+}/Fe^{2.5+}$**	**x**
10.6 nm	0	36	64	0.56	0.01
8.6 nm	0	40	60	0.67	0.04
5.3 nm	0	37	63	0.58	0.02

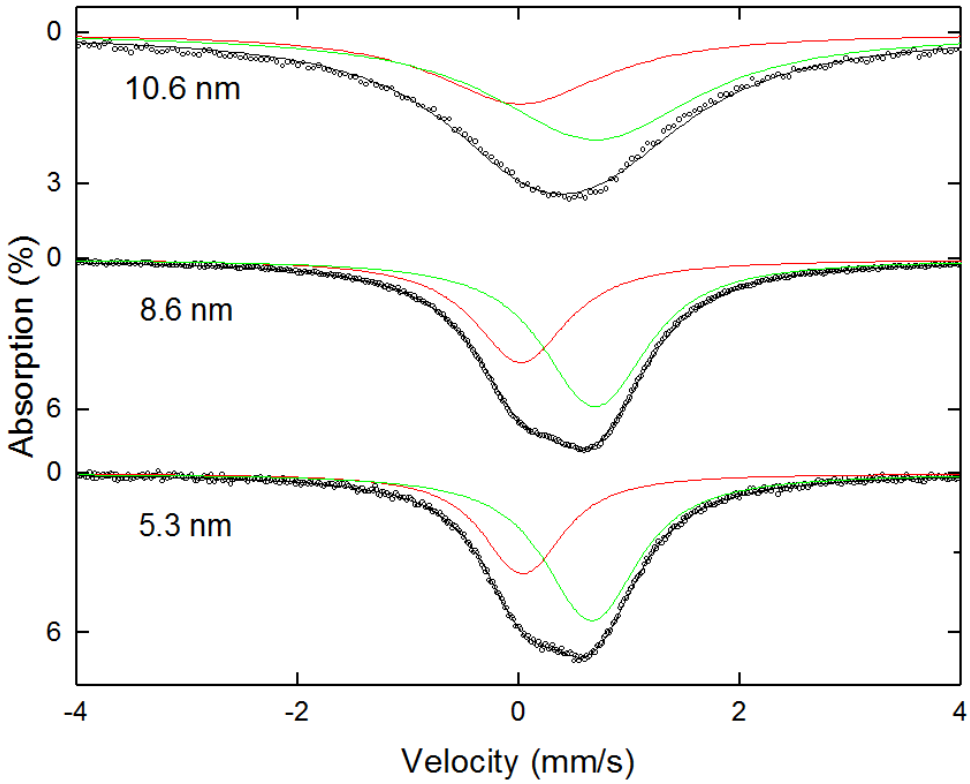


Figure 21 Mössbauer spectra of iron oxide nanoparticles, initial experiments at room temperature. The red lines indicate the tetrahedral site and the green is the octahedral.

Assuming the line with the smaller shift (red) and the one with the larger shift is the octahedral site (green) (due to the larger shift of the Fe^{2+} on the octahedral site), it is found here that the spectra can be fitted to fairly stoichiometric proportions, x being very close to zero.

This is not a common way to fit spectra of superparamagnetic samples at room temperature, since most investigators find more value in using the low temperature spectra.

The x values at room temperature confirm that the samples before oxidation are mostly stoichiometric, just as the x values at low temperature allow the same conclusion. Also, the 8.6 nm sample is consistently shown to be most non-stoichiometric, with the x values the largest for both methods. However, from this method, the 5.3 nm and 10.6 nm samples are harder to distinguish, with the difference being x = 0.01. Considering that their x-values at low temperature differ by a larger value, this likely signifies that there are larger errors for this model at room temperature. Additionally, the fitting of the 10.6 nm sample is less optimal than those of the 5.3 nm and 8.6 nm samples, mainly due to less asymmetry of the peak. This can account for the discrepancy of $x_{10.6} > x_{5.3}$ at low temperature but $x_{10.6} < x_{5.3}$ at room temperature. Although $x_{room} \neq x_{low}$ in all three cases, the x_{room}-values do show that the samples are mostly stoichiometric magnetite. This supports the idea that the Mössbauer spectra of superparamagnetic nanoparticles at room temperature have some value and the model here is a sound, though not fully accurate model. One caveat is that at room temperature, the Fe^{3+} percentages are slightly over-reported, since the Fe^{2+} recoilless fraction (f-factor, equation (7)) is smaller than the Fe^{3+} fraction at room temperature.

Magnetic Field Experiments

Since these nanoparticles are useful for MRI, it is important to investigate their behavior in a magnetic field. Coincidentally, this also helps in the studies relating to stoichiometry. The 10 kG and 20 kG experiments are presented.

Figure 22 shows the magnetite samples in 10 kG at room temperature, the key features being that the applied magnetic field has sharpened the lines, and for the 5.3 nm, 8.6 nm and 10.6 nm samples, the spectrum has been partially magnetized by the magnetic field and some of the different sites become distinguishable, much like the experiments done below the blocking temperature (Figure 19).

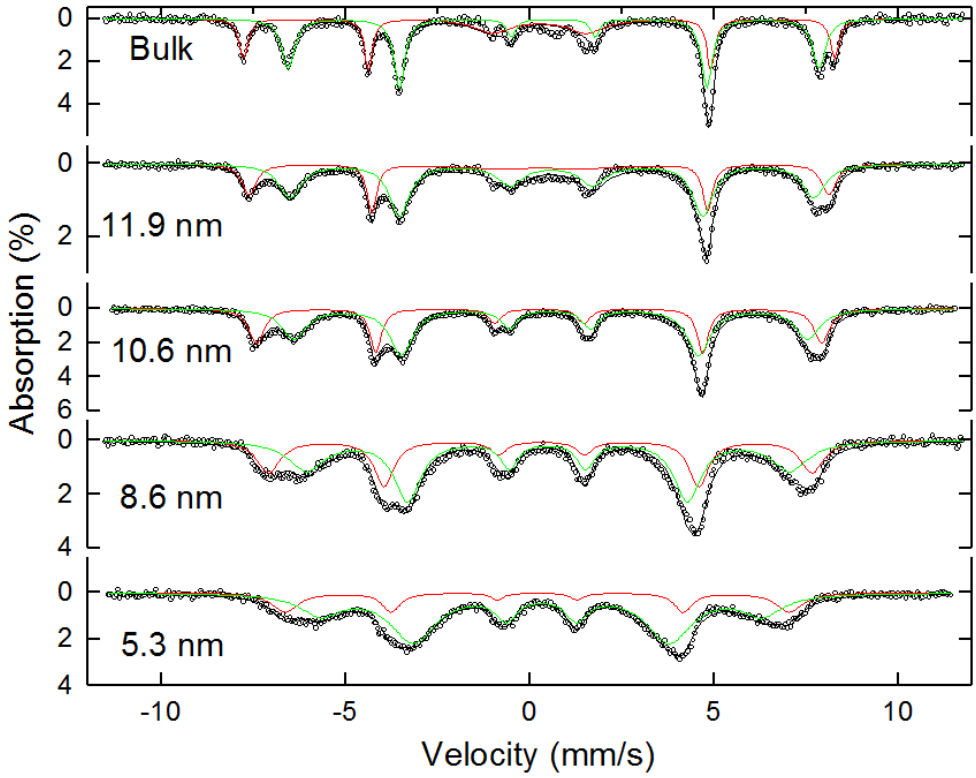


Figure 22 Mössbauer spectra of iron oxide nanoparticles, initial experiments in 10 kG magnetic field at room temperature.

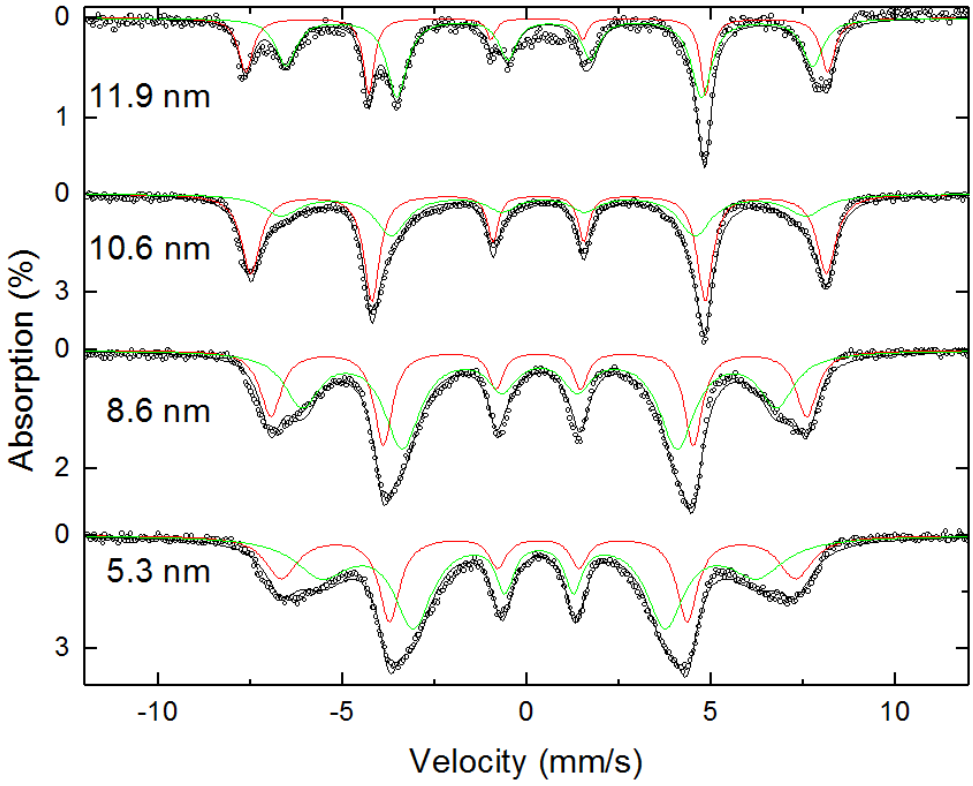


Figure 23 Mössbauer spectra of maghemite nanoparticles in 10 kG magnetic field at room temperature.

In addition, it can be noted that the smaller the sample, the broader the lines are, which could be attributed to the fact the smaller samples 'see' a smaller applied magnetic field, and are less magnetized. Smaller nanoparticles have a smaller total moment due to having lower number of magnetic moments; therefore, the hyperfine field strength is smaller as they are less aligned to the external magnetic field. This is also shown in the hyperfine field of the octahedral site (green lines), where the smaller samples have smaller octahedral site hyperfine fields. In 10 kG, only the 11.9 nm and 10.6 nm samples are confirmed to be mostly magnetite, with two distinct sites, whereas the stoichiometry of the smaller 5.3 nm and 8.6 nm samples are ambiguous in the magnetic field.

This is apparent when comparing the initial 10 kG experiments to those done three years later. Even though 5.3 nm nanoparticles are shown to be magnetite from experiments at low temperature, a comparison of the maghemite sample (Figure 23) and the magnetite experiments in 10 kG magnetic field show little obvious difference. This is due to the lines being broad in the 5.3 nm sample.

In the 10.6 nm sample however, after oxidation, the octahedral Fe^{2+} sites have been replaced by the octahedral Fe^{3+}, which being a similar species to the tetrahedral Fe^{3+} overlaps heavily. A closer inspection of the spectra for 10.6 nm particles initially (magnetite) and after three years (maghemite) is presented in Figure 24.

Since the 10 kG field seems inadequate in fully resolving the spectrum for the 5.3 nm nanoparticle, a stronger, 20 kG magnet was used. The field was applied to the magnetite samples and the experiments were repeated after three years (Figure 25 and Figure 26). In Figure 25, the 5.3 nm sample looks mostly resolved with distinct tetrahedral and octahedral lines, confirming this sample is mostly magnetite.

However, a closer observation of the initial samples in 20 kG show an unexpected site between the tetrahedral and the octahedral sites at the furthest left line (1^{st} line). This site is also not present in the bulk magnetite, which suggests that this site is unique to the nanoparticles.

All the nanoparticles show signs of this site, with the 11.9 nm sample being the least obvious. From the previous stoichiometric analysis, it was shown that the initial nanoparticles are not fully stoichiometric, but have some maghemite contamination.

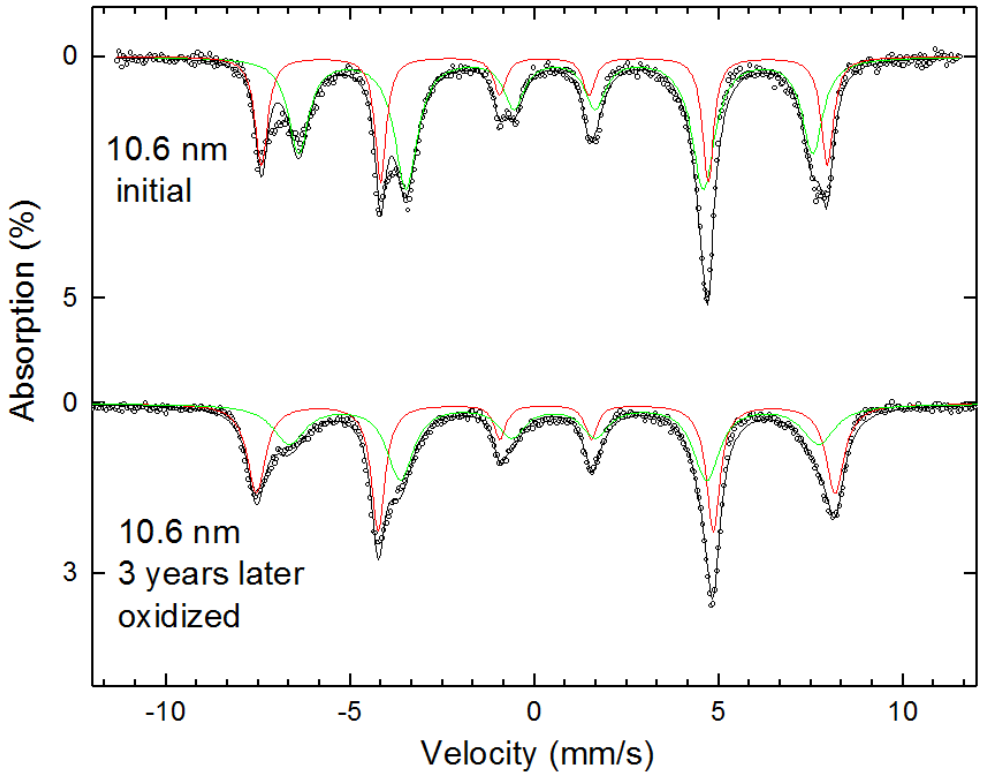


Figure 24 Mössbauer spectra of 10.6 nm sample in 10 kG magnetic field at room temperature.

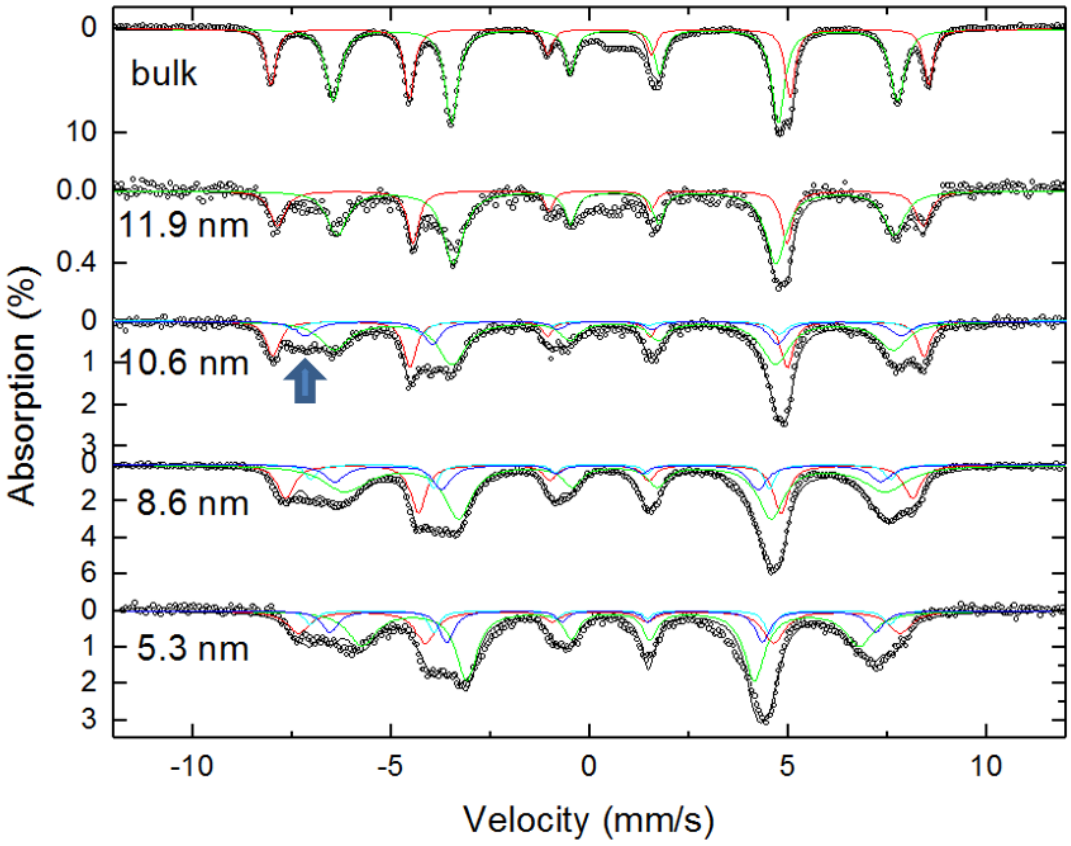


Figure 25 Mössbauer spectra of magnetite nanoparticles, initial experiments in 20 kG magnetic field at room temperature. The arrow points to the appearance of an unexpected site.

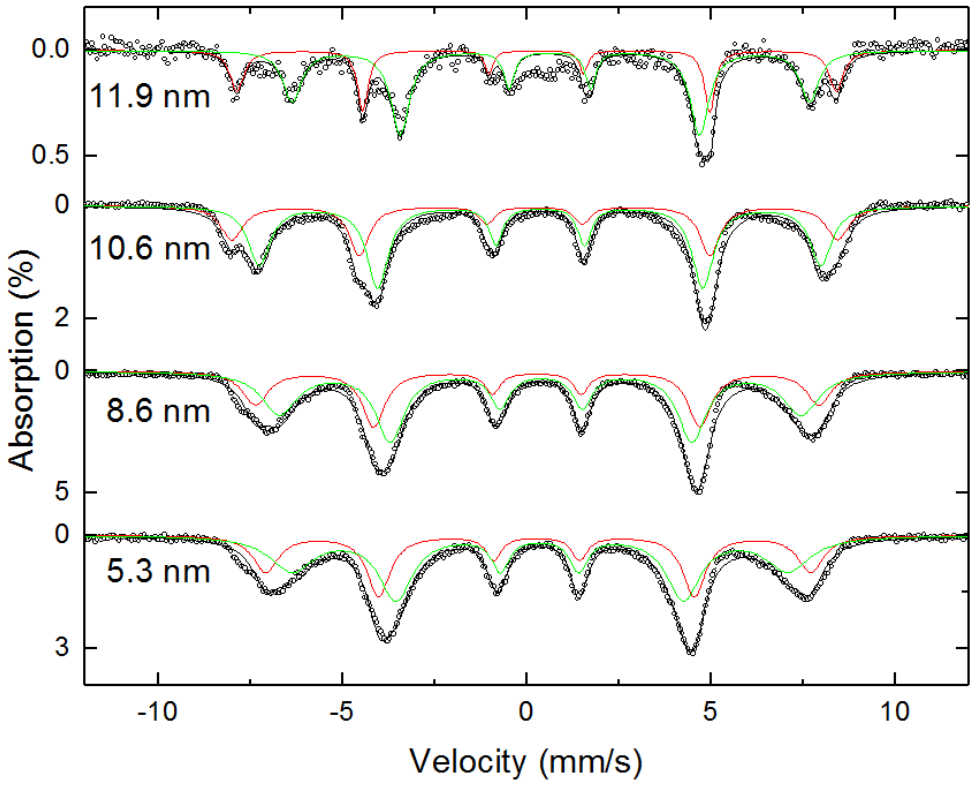


Figure 26 Mössbauer spectra of maghemite nanoparticles, in 20 kG magnetic field at room temperature.

This theory seems to be justified by Figure 27. The 1st tetrahedral line of the maghemite 10.6 nm sample matches up with the unexpected site (blue arrow) that is found from the initial sample, which means that the initial magnetite sample was already partially oxidized. Furthermore, upon closer inspection, another peak of this site (red arrow) at the 2nd line between the octahedral and tetrahedral sites of the magnetite sample also matches up to the 2nd tetrahedral line in the maghemite sample (Figure 27). The appearance of other maghemite peaks are not as obvious as they likely overlap with the peaks of the magnetite sample. These observations confirm earlier analysis that the initial magnetite nanoparticles are not 100% stoichiometric magnetite.

Magnetic Field Experiments: Stoichiometry

After performing the experiments in the magnetic field, the stoichiometry is obtained with the chemical formula $(Fe^{3+})_A[(Fe^{2.5+})_{2-6x}(Fe^{3+})_{5x}\square_x]_BO_4$. This is the appropriate since the experiments were done above the Verwey transition. Comparing the x values of the magnetic field and room temperature experiments negates the possibility of the f-factor as a source of error. The x values are presented in Table 4.

In Table 5, the obtained x values for room temperature, in magnetic field and low temperatures are compared. The x values obtained at all temperatures agree that the 8.6 nm magnetite nanoparticle is the most non-stoichiometric, since it has the biggest x value which corresponds to the most amount of oxidized Fe^{2+}. In addition, it is found that the x values at room temperature and in magnetic field agree for the 10.6 nm nanoparticles but not for the 8.6 nm and 5.3 nm nanoparticles. The x values in magnetic field show that the stoichiometry of the 5.3 nm and 10.6 nm cannot be differentiated at room temperature. The closeness of the x values at room temperature and magnetic field means that the room temperature fits are valid.

Table 4 In magnetic field percentages of iron species of initial samples.

	Applied field (kG)	**Fe^{3+}(%)**	**$Fe^{2.5+}$(%)**	**$Fe^{3+}/Fe^{2.5+}$**	**x**
10.6 nm	10	35	65	0.54	0.01
8.6 nm	10	37	63	0.59	0.02
5.3 nm	10	34	65	0.55	0.01

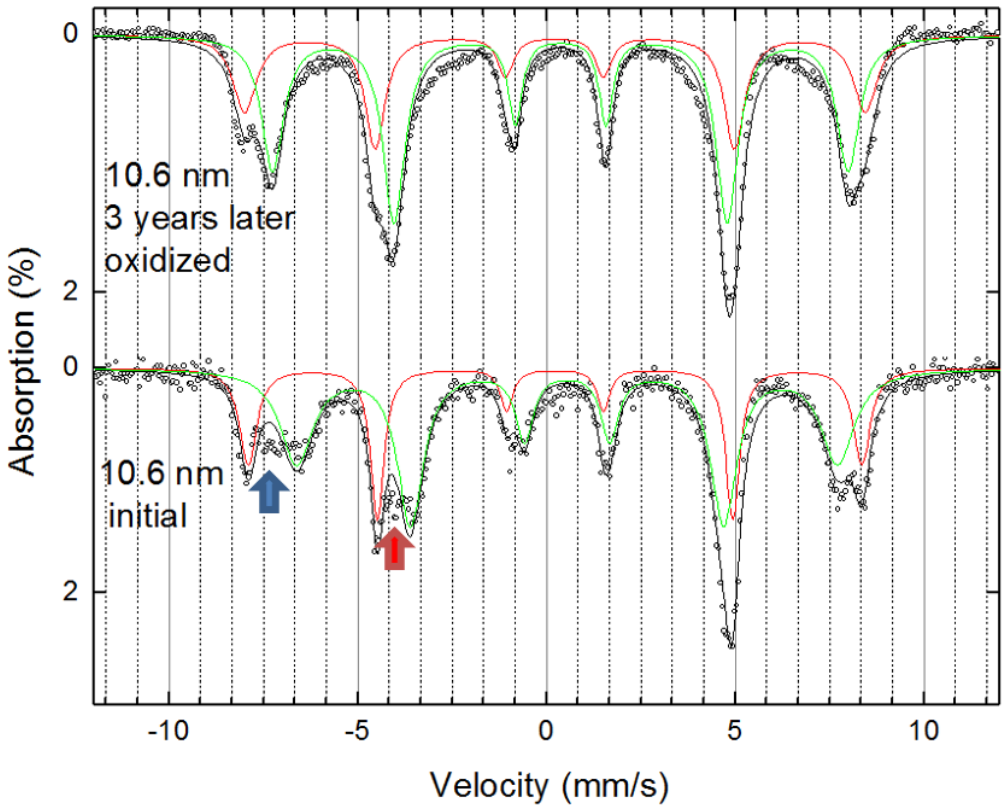


Figure 27 Mössbauer spectra of the 10.6 nm sample in 20 kG magnetic field at room temperature. The arrows point to the unexpected site. Note that the octahedral site on the maghemite sample lines up with the unexpected site at the areas where the arrows are pointing in the magnetite.

Table 5 Comparison of the x values for room temperature, in magnetic field and low temperature.

	x (room temperature)	**x (in magnetic field)**	**x (low temperature)**
10.6 nm	0.01	0.01	0.09
8.6 nm	0.04	0.02	0.12
5.3 nm	0.02	0.01	0.07

Blocking Temperature and Superparamagnetism

Given that the 5.3 nm, 8.6 nm and 10.6 nm samples seem fully oxidized into maghemite after three years, the blocking temperature could also be different. The 11.9 nm sample will not be discussed since its blocking temperature is above room temperature and is already 'blocked'.

The blocking temperature (T_B), is the temperature where the spectrum goes from being a singlet/doublet to Zeeman split.

To determine where this temperature is, the Mössbauer spectra of the magnetite samples before oxidation as a function of varying temperature is presented in Figure 28. The blocking temperature is not incredibly well defined visually, but typically taken to be the point where the hyperfine field becomes visible and distinct, hence the blocking temperature is approximate when observed visually. This will be corroborated with motional narrowing methods later in the discussion. However, there is an added complication that the peaks can be very broad even after being blocked.

For samples 5.3 nm and 10.6 nm the lines start becoming distinct around 50 K and 125 K respectively. The 8.6 nm sample unfortunately has a noisier spectrum, so visually 50-100 K seems to be where the blocking temperature is.

The blocking temperature in descending order of nanoparticle size makes sense as the smaller the volume of nanoparticle, the faster the relaxation time at a particular temperature, therefore it has a lower blocking temperature (equation 5).

In the maghemite samples (Figure 29), the blocking temperature does not seem to have changed much, with the 5.3 nm sample being blocked around 55 K; 8.6 nm at around 85 K; and 10.6 nm around 180 K.

To conclude, the blocking temperature seems to increase slightly (~10 K) when the stoichiometry changes in the nanoparticles, which means the more deterministic factor for the blocking temperature is the particle's volume/size.

Relaxation Time: A Motional Narrowing Analysis

To find the characteristic relaxation time, τ_0, motional narrowing analysis is used. Relaxation time is an important parameter in MRI. Motional narrowing is well understood in NMR, however, it is less explored with Mössbauer spectroscopy.

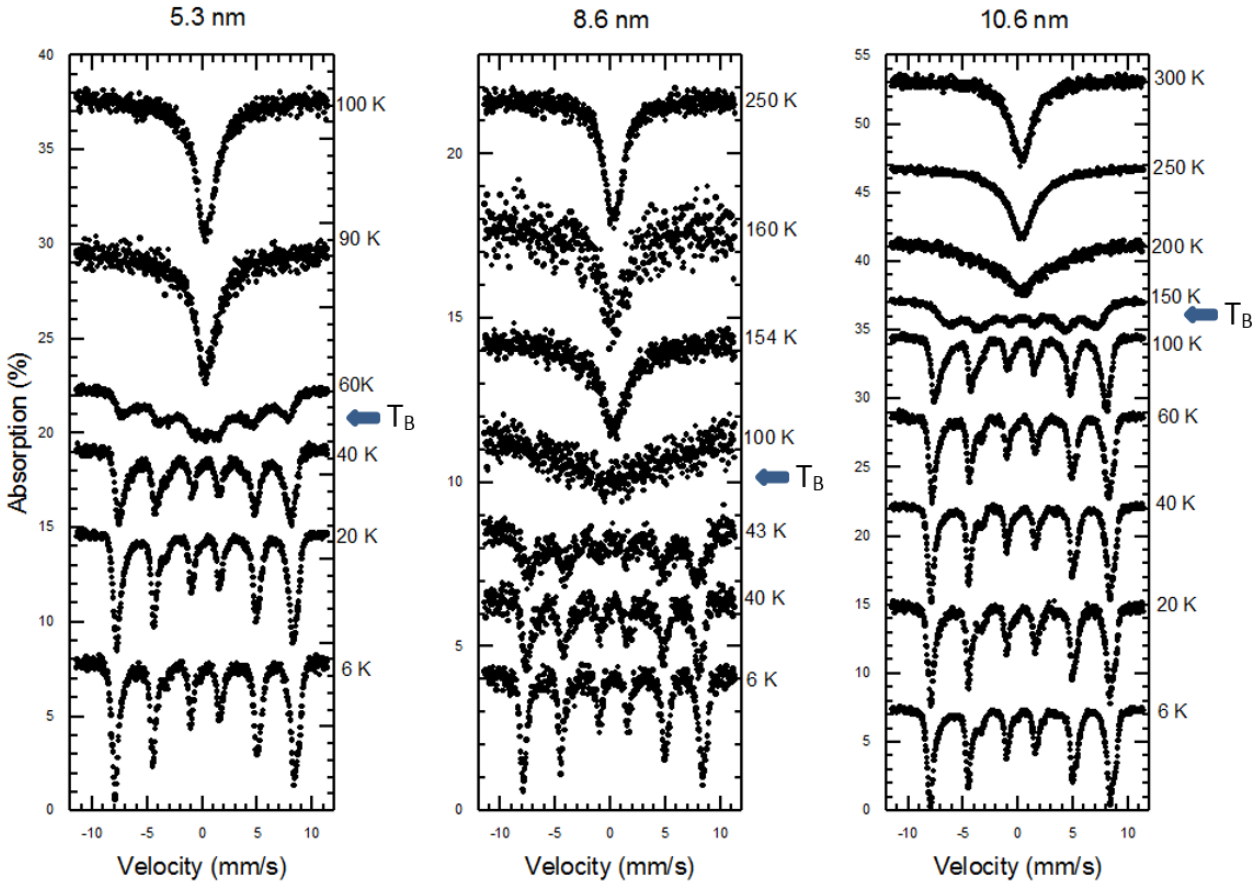


Figure 28 The initial varying temperature experiments of magnetite samples 5.3 nm, 8.6 nm and 10.6 nm.

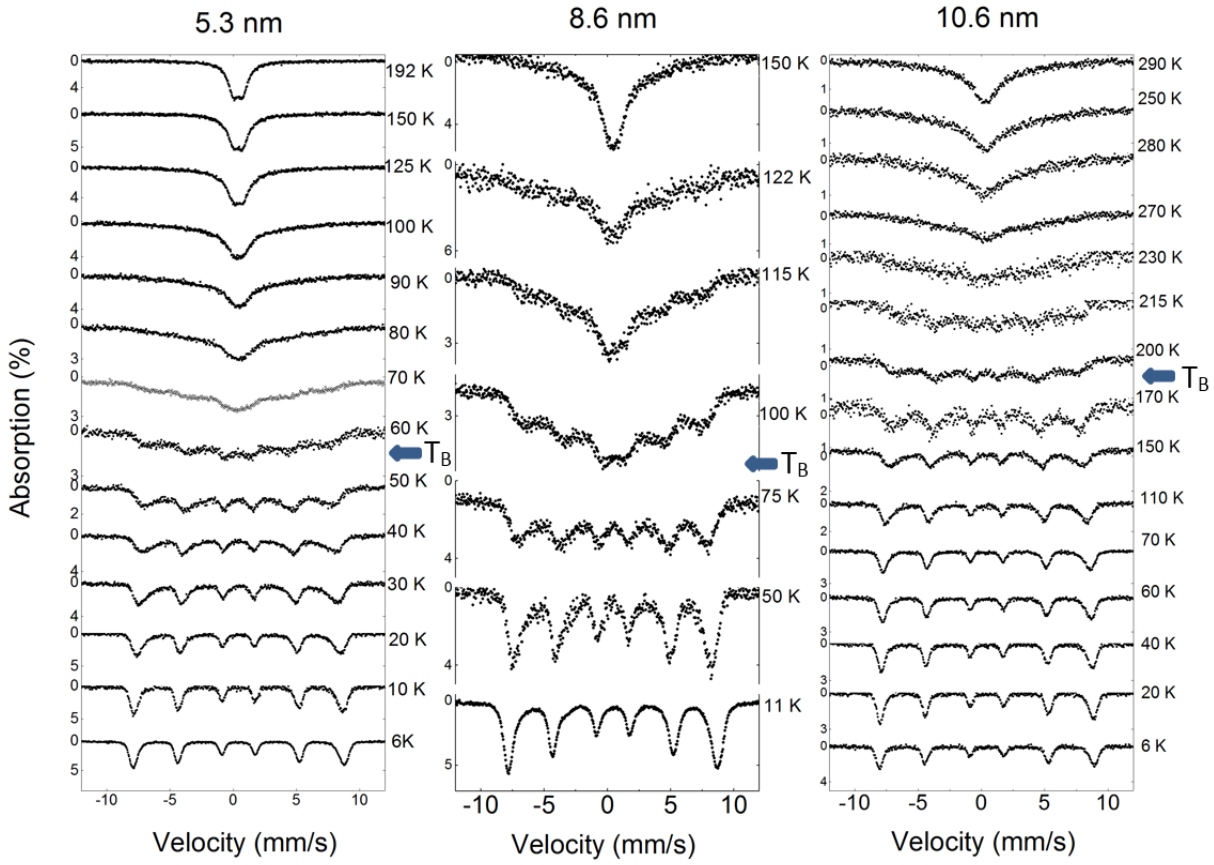


Figure 29 The varying temperature experiments of maghemite samples 5.3 nm, 8.6 nm and 10.6 nm.

This is the method that will be used to investigate the relaxation time. Motional narrowing, as mentioned earlier, is a method to investigate line-narrowing as the temperature is increased, which is related to the relaxation time by equation (9). The nanoparticle spectra start out as a single line and broaden as the temperature is decreased. Below the blocking temperature, the spectra splits and shows a hyperfine field. Since the spectra below the blocking temperature are complicated with overlapping lines, the linewidths are not easy to determine. As a result, only the spectra above the blocking temperature will be discussed. This excludes the 11.9 nm sample since it does not have a blocking temperature below room temperature.

For the smaller maghemite samples (5.3 nm and 8.6 nm), the room temperature spectra presents a symmetrical doublet with a quadrupole splitting of about 0.7 mms^{-1}, making the fit straightforward.

The quandary comes in the fitting of the 10.6 nm nanoparticle spectra. There are several factors to consider. Depending on whether there is one broad singlet or a doublet with a very small quadrupole splitting, the linewidth can be different. A further consideration is that there is a possibility that the quadrupole splitting can change as the temperature changes, which could be masked by the broadening of the linewidths.

Fitting and analyzing the spectra using motional narrowing has increased value because of the above-mentioned issues. Using equation (9), the parameter that is considered is the difference in the linewidths ($\Delta\Gamma$), not the absolute linewidths. As long as a fitting regime is selected and consistently applied, the results can still be of value. The initial unoxidized magnetite samples are fitted with a single peak, and the maghemite samples with a quadrupole splitting, to simplify the analysis. The spectra have at least two sources of broadening (hyperfine field and temperature broadening). Inhomogeneous broadening can be better fitted with a Voigt profile in NMR spectra[38]. As a result, a Voigt profile, which contains both Gaussian and Lorentzian profiles is the most appropriate for the Mössbauer fits as well. However, since the line shape of interest is the Lorentzian profile, which is the classic Mössbauer line shape, only the Lorentzian linewidth extracted from the Voigt profile will be discussed. With the Zeeman splitting occurring closer to the blocking temperature, additional sources of broadening are introduced. As a result, selecting the appropriate measurement temperatures is important. For the smaller samples, since the blocking temperature is much lower than room temperature, the experimental temperatures are in

larger increments. With the 10.6 nm sample however, the blocking temperature is higher and the experimental increments are smaller.

Assumptions

A few assumptions are made during the application of this method. It is assumed that the Lorentzian portion of the linewidths are only broadened due to the increase of the average "seen" magnetic field. Additional sources of broadening introduced when close to the blocking temperature is assumed to be captured by the Gaussian portion of the Voigt function.

Another assumption made is that the instantaneous field strength is the same across all experimental temperatures. It is known that this is not completely true. The hyperfine field does vary as the temperature changes. However, allowing the field to be constant simplifies the analysis. Here the hyperfine field is taken to be 500 kG across the temperatures used for this method.

Analysis

The $\Delta\Gamma$ used in equation (9) is found by subtracting the measured linewidth from the linewidth assumed to be from experimental broadening and natural linewidth (taken to be 0.3 mms^{-1}). The linewidth is then converted to angular frequency, with ω taken to be 10^9 s^{-1} (based on a magnetic field of 500 kG). The results are presented in Table 6.

Unsurprisingly, the table shows that the lower the experiment temperature the slower the relaxation time of the nanoparticles, corresponding to the increased broadening. For the 5.3 nm and 8.6 nm samples, the relaxation times are comparable both for magnetite and maghemite samples, around 10^{-11}s. The 10.6 nm sample has both maghemite and magnetite components with relaxation times in the region of 10^{-10}s. This fits with the trend that the larger the nanoparticles, the slower the relaxation time. After the individual relaxations are found for each temperature, equation (4) is rearranged to find the characteristic relaxation time. Rearranging equation (4):

$$ln\,\tau = \frac{KV}{kT} + ln\,\tau_0 \qquad (10)$$

By plotting $ln\,\tau$ against *1/T*, the value of the slope, $\frac{KV}{kT}$, is found. The y-intercept, $ln\,\tau_0$, is shown in Table 7. As this is an uncommon approach to finding the relaxation time, to check that the values obtained are reliable, an estimate of the blocking temperature using equation (5) is done.

Table 6 Nanoparticle relaxation times.

Particle size (nm)	**Temperature (K)**	**Linewidth Γ (mms^{-1})**	**Relaxation Time τ (s)**
5.3	293	0.73	2.32×10^{-11}
	200	0.85	2.96×10^{-11}
	150	1.35	5.66×10^{-11}
5.3 (oxidized)	293	0.96	3.55×10^{-11}
	192	1.13	4.47×10^{-11}
	150	1.47	6.30×10^{-11}
8.6	293	0.92	3.34×10^{-11}
	250	2.13	9.86×10^{-11}
	160	2.83	1.36×10^{-10}
8.6 (oxidized)	293	0.89	3.18×10^{-11}
	250	1.23	5.01×10^{-11}
	220	1.36	5.71×10^{-11}
10.6	300	2.36	1.11×10^{-10}
	250	3.13	1.52×10^{-10}
	200	6.5	3.34×10^{-10}
10.6 (oxidized)	293	3.41	1.68×10^{-10}
	280	4.61	2.32×10^{-10}
	270	5.48	2.79×10^{-10}

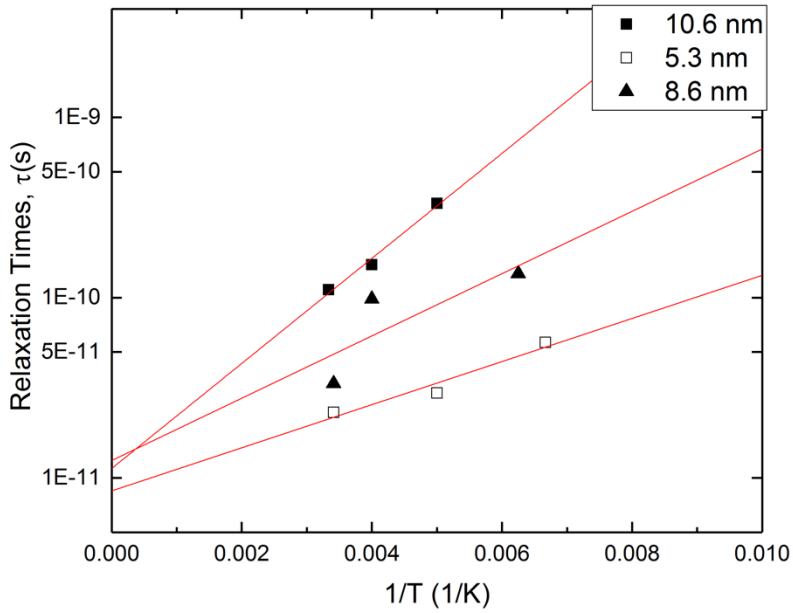


Figure 30 Plot of ln τ against 1/T for initial unoxidized magnetite 5.3 nm, 8.6 nm and 10.6 nm nanoparticles.

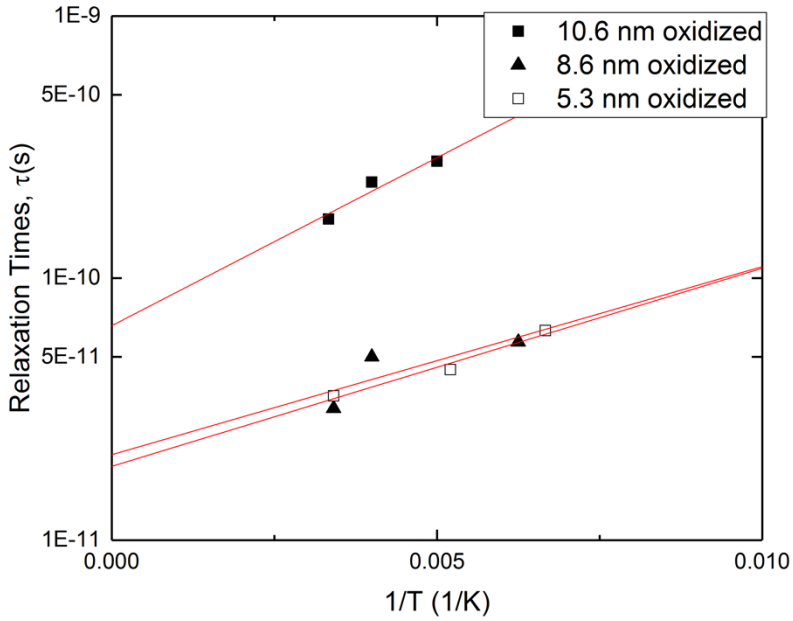


Figure 31 Plot of ln τ against 1/T for maghemite 5.3 nm, 8.6 nm and 10.6 nm nanoparticles.

Table 7 The characteristic relaxation times and blocking temperature of the particles.

Particle size (nm)	**Relaxation Time τ_0 (s)**	**Derived Blocking Temperature (K)**	**Experimental blocking temperature (K)**
5.3	8.48×10^{-12}	50	50
5.3 (oxidized)	5.95×10^{-12}	51	55
8.6	2.11×10^{-11}	90	between 50 and 100
8.6 (oxidized)	5.64×10^{-12}	77	85
10.6	1.14×10^{-11}	110	125
10.6 (oxidized)	4.21×10^{-12}	187	180

From Table 7, the derive blocking temperatures of the magnetite and maghemite 5.3 nm nanoparticles match closely to the experimental ones. For maghemite 8.6 nm samples, the values also match closely, and the derived blocking temperature for the magnetite sample falls within the experimental range of the blocking temperature.

However, the 10.6 nm sample, for both magnetite and maghemite there is greater variation between the derived and experimental blocking temperature. The errors of fitting are larger due to being closer to the blocking temperature and there are more sources of broadening. In addition, the blocking temperature is higher for the maghemite samples.

Otherwise, it can be concluded that for samples that have blocking temperatures much lower than room temperature, the motional narrowing method seems a reasonable method to derive the relaxation time and the blocking temperature. However, for samples with blocking temperatures closer to room temperatures, like samples larger than 10 nm have, this method will be approximate.

Motional Narrowing: Limitations

There are limitations to this approach, samples where the blocking temperature is above room temperature cannot be analyzed, since the hyperfine field for these samples are not collapsed. A lower bound for the relaxation time for these samples can be set, since they have to be slower than the measurement time of Mössbauer spectroscopy (5×10^{-9} s). Since the motional narrowing method

cannot be applied to the 11.9 nm sample (there is no blocking temperature), it can be assumed the method only allows the estimation of relaxation times of magnetite/maghemite samples with sizes below 11.9 nm.

Chapter 4 Conclusion

In summary, the stoichiometry of magnetite superparamagnetic iron oxide nanoparticles were characterized with Mössbauer spectroscopy. The experiments were repeated three years later. To evaluate the stoichiometry, the fitted spectra were compared to the ideal stoichiometric chemical formulae, $(Fe^{3+})_A[(Fe^{2+})_{1-3x}(Fe^{3+})_{1+2x}\square_x]_BO_4$, for low temperature experiments (mainly 5 K), and $(Fe^{3+})_A[(Fe^{2.5+})_{2-6x}(Fe^{3+})_{5x}\square_x]_BO_4$ for room temperature experiments.

While the fitting for low temperature experiments are well-established, the fitting for spectra of superparamagnetic magnetite nanoparticles at room temperature is rarely done. Here, the superparamagnetic asymmetric singlets were fitted similar to magnetite above the Curie temperature. The assumptions for the model is derived from similarities in the spectra transitioning across the Curie temperature and blocking temperature. The fitted results from the model was found to be valid and its accuracy confirmed by comparison of the stoichiometry at room and low temperature. This is important because the MRI SPION contrast agents will be used in ambient atmosphere, which can oxidize if magnetite.

Understanding the relaxation time is also important in MRI. While motional narrowing is very common in NMR, there has been very little done using it to find relaxation times in Mössbauer spectroscopy. By observing motional narrowing in Mössbauer spectroscopy, relaxation times were derived. In all but one sample, the derived blocking temperature compares well to the experimental one. The derived blocking temperature of the 10.6 nm sample is suspected to have greater fitting errors due to the spectra not being completely Lorentzian and having multiple sources to the linewidth broadening. As a result, the derived blocking temperature deviates more from the experimental one.

Finally, it is found that the blocking temperature is approximately the same after oxidation of the magnetite nanoparticles into maghemite. This points to the importance of the size of the nanoparticle being the overwhelming factor in the blocking temperature, since oxidation of the nanoparticles do not modify their size.

References

1. Donya Ramimoghadam, Samira Bagheri, Sharifah Bee Abd Hamid. Progress in electrochemical synthesis of magnetic iron oxide nanoparticles, *Journal of Magnetism and Magnetic Materials*, volume 368, pages 207 - 229
2. P. Kucheryavy, J. He, V.T. John, P. Maharjan, L. Spinu, G.Z. Goloverda, V.L. Kolesnichenko, Superparamagnetic iron oxide nanoparticles with variable size and an iron oxidation state as prospective imaging agents, *Langmuir : the ACS Journal of Surfaces and Colloids*, 29 (2013) 710-716.
3. Strehl C, Gaber T, Maurizi L, et alet al. Effects of PVA coated nanoparticles on human immune cells. *International Journal of Nanomedicine*. 2015;10:3429-3445.
4. L. Theil Kuhn and A. Bojesen and L. Timmermann and K. Fauth and E. Goering and E. Johnson and M. Meedom Nielsen and S. Mørup. Core-shell iron–iron oxide nanoparticles: magnetic properties and interactions. *Journal of Magnetism and Magnetic Materials*, volume 272-276, pages1485 – 1486, 2004.
5. Mahmoudi M, Simchi A, Milani AS, Stroeve P. Cell toxicity of superparamagnetic iron oxide nanoparticles. *Journal of Colloid and Interface Science*. 2009;336(2):510-8.
6. Li L, Jiang W, Luo K, Song H, Lan F, Wu Y et alet al. Superparamagnetic Iron Oxide Nanoparticles as MRI contrast agents for Non-invasive Stem Cell Labeling and Tracking. *Theranostics*. 2013;3(8):595-615.
7. R. Hergt, S. Dutz, R. Müller, M. Zeisberger, Magnetic particle hyperthermia: nanoparticle magnetism and materials development for cancer therapy, *Journal of Physics: Condensed Matter*, 18 (2006) S2919-S2934.
8. Sillerud LO, Solberg NO, Chamberlain R, et alet al. SPION-Enhanced Magnetic Resonance Imaging of Alzheimer's Disease Plaques in AβPP/PS-1 Transgenic Mouse Brain. *Journal of Alzheimer's disease : JAD*. 2013;34(2):349-365. doi:10.3233/JAD-121171.
9. Health, United States, 2016. Centers for Disease Control and Prevention. 2016. https://www.cdc.gov/nchs/data/hus/hus16.pdf. 2017.
10. Na HB, Song IC, Hyeon T. Inorganic Nanoparticles for MRI Contrast Agents. *Advanced Materials*. 2009;21(21):2133-48.
11. Oshtrakh MI, Ushakov MV, Šepelák V, Semionkin VA, Morais PC. Study of Iron oxide nanoparticles using Mössbauer spectroscopy with a high velocity resolution. *Spectrochimica Acta Part A: Molecular and Biomolecular Spectroscopy*. 2016;152(Supplement C):666-79.
12. Woo K, Hong J, Choi S, Lee H-W, Ahn J-P, Kim CS et alet al. Easy Synthesis and Magnetic Properties of Iron Oxide Nanoparticles. *Chemistry of Materials*. 2004;16(14):2814-8.
13. Santoyo Salazar J, Perez L, de Abril O, Truong Phuoc L, Ihiawakrim D, Vazquez M et alet al. Magnetic Iron Oxide Nanoparticles in 10−40 nm Range: Composition in Terms of Magnetite/Maghemite Ratio and Effect on the Magnetic Properties. *Chemistry of Materials*. 2011;23(6):1379-86.
14. Lodhia J, Mandarano G, Ferris NJ, Eu P, Cowell SF. Development and use of iron oxide nanoparticles (Part 1): Synthesis of iron oxide nanoparticles for MRI. *Biomedical Imaging and Intervention Journal*. 2010;6(2):e12.
15. Oshtrakh MI, Ushakov MV, Šepelák V, Semionkin VA, Morais PC. Study of Iron oxide nanoparticles using Mössbauer spectroscopy with a high velocity resolution.

Spectrochimica Acta Part A: Molecular and Biomolecular Spectroscopy. 2016;152 (Supplement C):666-79.
16. Hah H-Y. Magnetism of Magnetite nanoparticles as determined by Mössbauer Spectroscopy: *University of Tennessee*; 2016.
17. B. T. Draine and Brandon Hensley. Magnetic Nanoparticles in the Interstellar Medium: Emission Spectrum and Polarization, *The Astrophysical Journal*, volume 765, 2, pages 159, 2013.
18. B.J. Evans, 57Fe Hyperfine Fields in Magnetite (Fe_3O_4), *Journal of Applied Physics*, 40, 1969, 1411.
19. J.M. Zuo, J.C.H. Spence, Charge ordering in magnetite at low temperatures, *Physical Review B*, 42, 1990, 8451-8464.
20. J. García, G. Subías, The Verwey transition—a new perspective, *Journal of Physics: Condensed Matter*, 16 (2004) R145-R178.
21. G.A. Sawatzky, Mössbauer Study of Electron Hopping in the Octahedral Sites of Fe_3O_4, *Journal of Applied Physics*, 40 (1969) 1402.
22. M. Jackson, B. Moskowitz, J. Bowles, Interpretation of Low-Temperature Data Part III:The Magnetite Verwey Transition, *The IRM Quarterly*, 2011, 20.
    A. Gedikoǧlu, Mössbauer study of low temperature oxidation in natural magnetite, *Scripta Metallurgica*, Volume 17, Issue 1, 1983, Pages 45-48.
23. Florez, J. M., Mazo-Zuluaga, J. and Restrepo, J., Ferrimagnetic to Paramagnetic Transition in Magnetite: Mössbauer versus Monte Carlo, *Hyperfine Interactions*, 2005, volume 161, pages 161-169.
24. E. Lima, A.L. Brandl, A.D. Arelaro, G.F. Goya, Spin disorder and magnetic anisotropy in Fe_3O_4 nanoparticles, *Journal of Applied Physics*, 99 (2006) 083908.
25. S.H. Kilcoyne, Ferritin: a model superparamagnet, *Journal of Magnetism and Magnetic Materials* 140-144 (1995) 1466-1467.
26. Sobolev, A. V., Presnyakov, I. A., Rusakov, V. S., Gapochka, A. M., Glazkova, Ya. S., Matsnev, M. E., and Pankratov, D. A., Mössbauer study of the modulated magnetic structure of $FeVO_4$, Journal of Experimental and Theoretical Physics, 2017, volume 124, pages 943—956.
27. G.K. Wertheim, Mössbauer effect: principles and applications, Academic Press, 1964.
28. Pines, David and Slichter, Charles P., Relaxation Times in Magnetic Resonance, *Physical Review*, volume 100, 1955, pages 1014-1020.
29. Galina Goloverda, Barry Jackson, Clayton Kidd, Vladimir Kolesnichenko, Synthesis of ultrasmall magnetic iron oxide nanoparticles and study of their colloid and surface chemistry, *Journal of Magnetism and Magnetic Materials*, Volume 321, Issue 10, 2009, Pages 1372-1376.
30. Christine Rümenapp, Friedrich E. Wagner, Bernhard Gleich, Monitoring of the aging of magnetic nanoparticles using Mössbauer spectroscopy, *Journal of Magnetism and Magnetic Materials*, Volume 380, 2015, Pages 241-245.
31. Christopher A. Gorski, Michelle M. Scherer; Determination of nanoparticulate magnetite stoichiometry by Mössbauer spectroscopy, acidic dissolution, and powder X-ray diffraction: A critical review. *American Mineralogist* ; 95 (7): 1017–1026.
32. Zakharova, I. N. Shipilin, M. A. and Alekseev, V. P. and Shipilin, A. M. Mössbauer study of maghemite nanoparticles, *Technical Physics Letters*, 2012, Volume 38, pages 55-58.

33. Frank J Berry, Steven Skinner and Michael F Thomas, Mössbauer spectroscopic examination of a single crystal of Fe_3O_4, *Journal of Physics: Condensed Matter*, 1998, Volume 10, pages 215
34. Kosterov, Andrei. Magnetic properties, low-temperature. In Gubbins, David; Herrero-Bervera, Emilio. Encyclopedia of geomagnetism and paleomagnetism. *Dordrecht: Springer*. 2007. pp. 515–525.
35. Alexander Joos, Christine Rümenapp, Friedrich E. Wagner, Bernhard Gleich, Characterisation of iron oxide nanoparticles by Mössbauer spectroscopy at ambient temperature, *Journal of Magnetism and Magnetic Materials*, Volume 399, 2016, Pages 123-129
36. Persoons, R. M. and De Grave, E. and de Bakker, P. M. A. and Vandenberghe, R. E., Mössbauer study of the high-temperature phase of Co-substituted magnetites, *Physical Review B*, volume 47, issue 10, 1993, pages 5894-5905.
37. Stephen D Bruce, John Higinbotham, Ian Marshall, Paul H Beswick, An Analytical Derivation of a Popular Approximation of the Voigt Function for Quantification of NMR Spectra, *Journal of Magnetic Resonance*, volume 142, Issue 1, 2000, pages 57-63.

Vita

Hien-Yoong Hah grew up in Malaysia and attended higher education at Coe College, in Cedar Rapids, Iowa. After that he was fortunate to be accepted into graduate school at University of Tennessee Space Institute, Tullahoma, Tennessee. He obtained his masters from said institution, and proceeded to complete his doctoral work in the same institution. Much of what he achieved was done with huge amounts of help and support from friends, colleagues, advisors, family and most importantly his parents.